Difficult/Remaining Issues in Atmospheric Correction of Ocean Color Imagery

Robert Frouin
Scripps Institution of Oceanography
8810 Shellback Way, La Jolla, California
rfrouin@ucsd.edu

2023 Ocean Optics Summer Course, 12 June – 7 July 2023, Bowdoin College, Schiller Coastal Studies Center (SCSC), Orr's Island, Maine

Issues

1. Absorbing aerosols

2. Whitecaps

3. Adjacency effects

4. Clouds/Sun glint

(For a discussion of these and other atmospheric correction issues, see: Frouin et al., 2019, Atmospheric correction of ocean color imagery during the PACE era, *Front. Earth Sci. 7:145,* doi: 10.3389/feart.2019.00145.)

1. Absorbing Aerosols

Introduction

-Absorbing aerosols are particles that have a refractive index with a non-null imaginary part. In terms of radiation transfer, their single scattering albedo (i.e., the ratio of scattering and extinction coefficients), ω_{aer}, is less than 1.

-There are two basic sources of absorbing aerosols, both of terrestrial origin:

(i) Industrial, as a soot component of small particles present in variable amount in urban-type aerosols, and

(ii) Natural, as small or large mineral particles present in desert dust aerosols.

GEOS Model Aerosol Simulations, Sep-Oct 2006

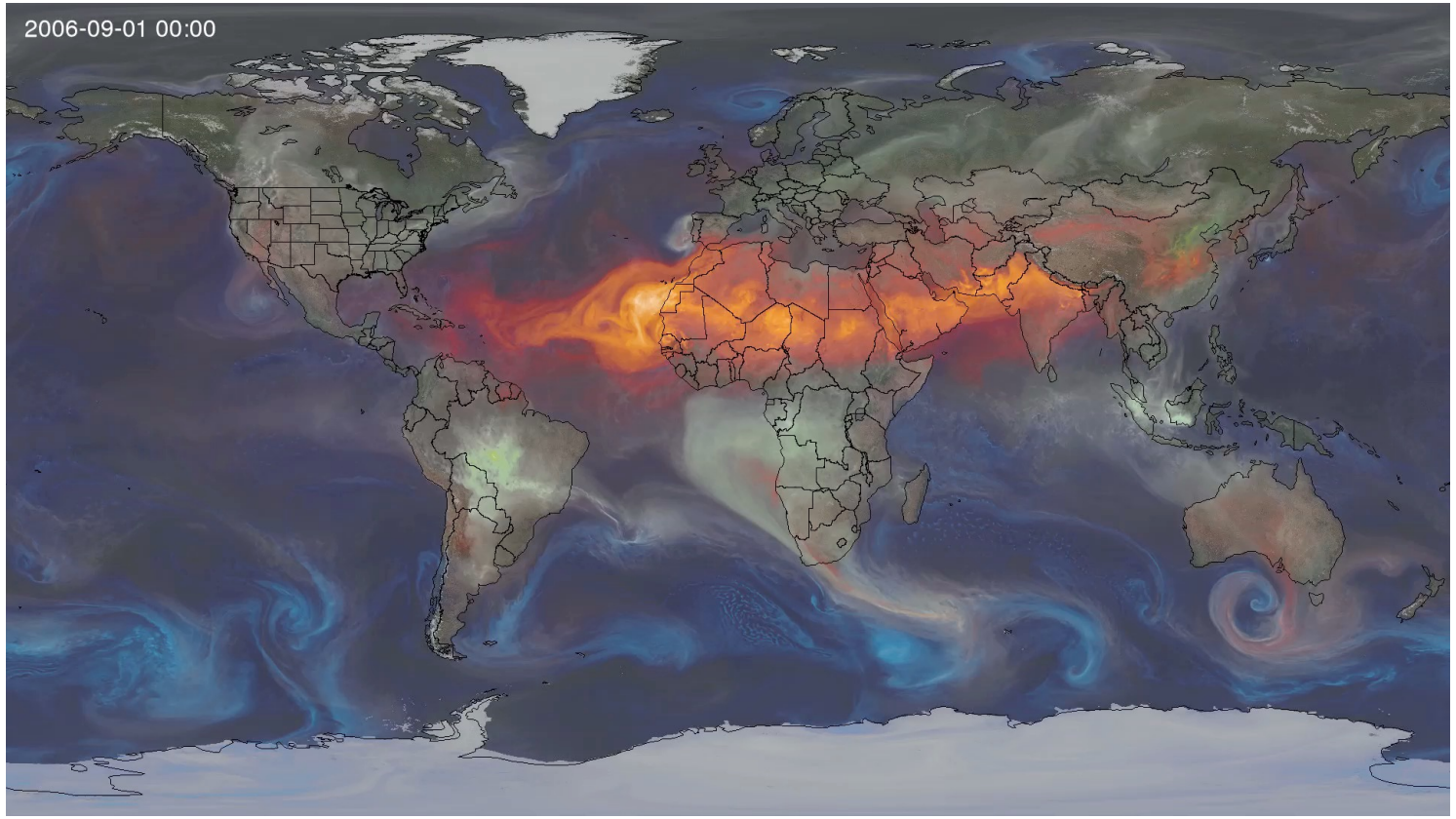

***Figure 1-1**: Global 10km resolution aerosol simulations from GEOS model, v5. Time period is September-October 2006. The model is driven by observed sea surface temperature and daily fire emissions derived from MODIS fire radiative power. Dust, sea-salt, and carbonaceous aerosols are displayed in orange, blue, and green tones, respectively. (Arlindo Silva, NASA GSFC, 2012.)*

-Absorbing aerosols affect large oceanic areas, not just the coastal one.

Aerosol absorption effect

-Aerosol scattering affects the TOA reflectance at all wavelengths. It is better detected as a TOA reflectance increase with decreasing wavelength at large wavelengths, above 700 nm where the ocean reflectance is null or small.

-Aerosol absorption does influence strongly the TOA reflectance at ocean color wavelengths, especially in the blue and ultraviolet, where it constitutes a source of error for ocean-color retrievals.

-The effect of aerosol absorption is mainly the result of its interaction with molecular scattering. It depends on the absorption optical thickness and the location of the aerosol layer in the vertical, and it increases with the altitude of the aerosol layer. It can be written (Torres, 2002):

$$\rho_{a\_abs} \approx -(1 - \omega_{aer})\tau_{aer}\, m^*[\rho_w T_a + \rho_{mol}(P_s - P_a)/P_s]$$

Aerosol absorption effect

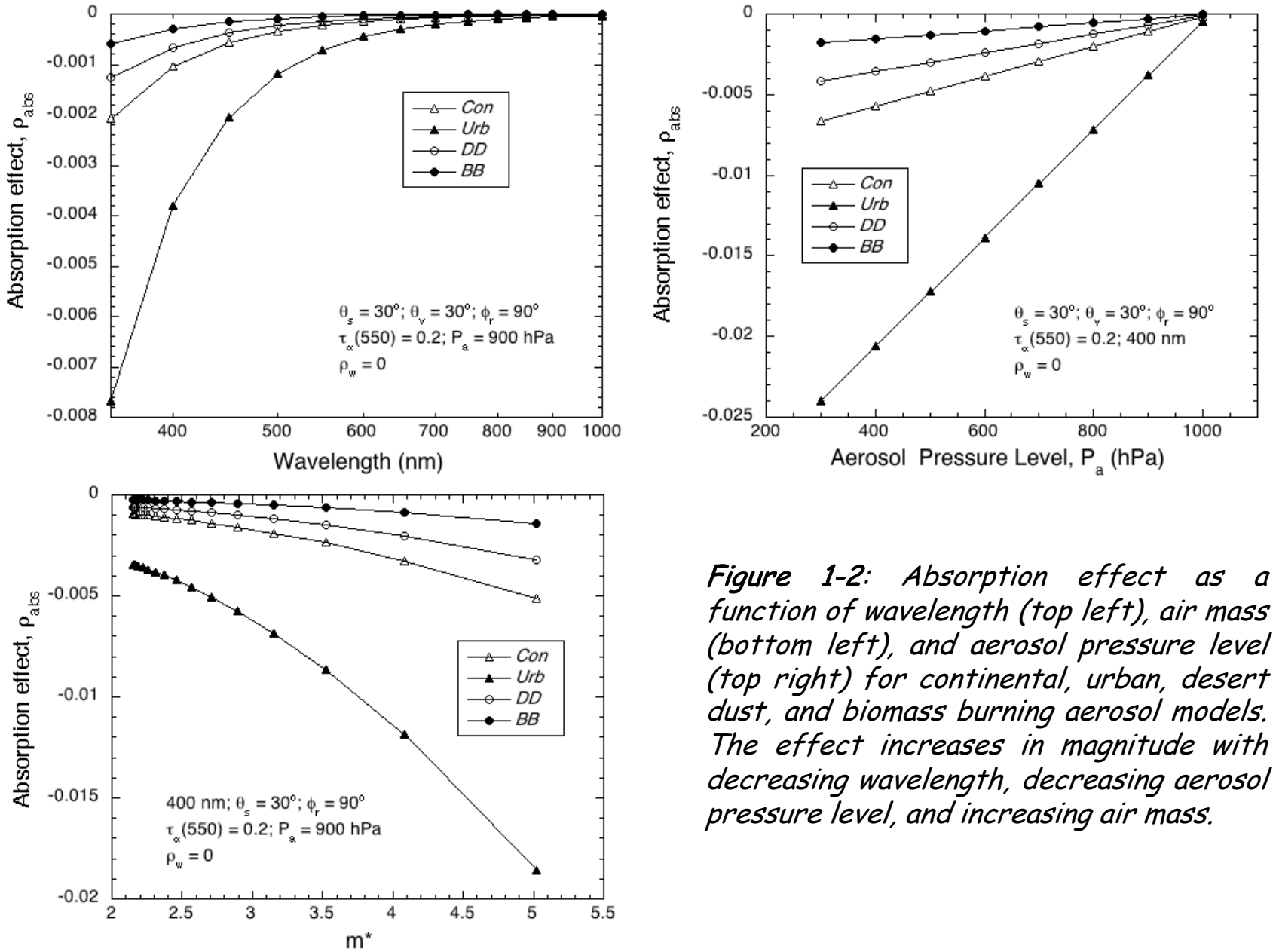

Figure 1-2: *Absorption effect as a function of wavelength (top left), air mass (bottom left), and aerosol pressure level (top right) for continental, urban, desert dust, and biomass burning aerosol models. The effect increases in magnitude with decreasing wavelength, decreasing aerosol pressure level, and increasing air mass.*

Dust storm out of Libya, 20 June 1997, POLDER imagery

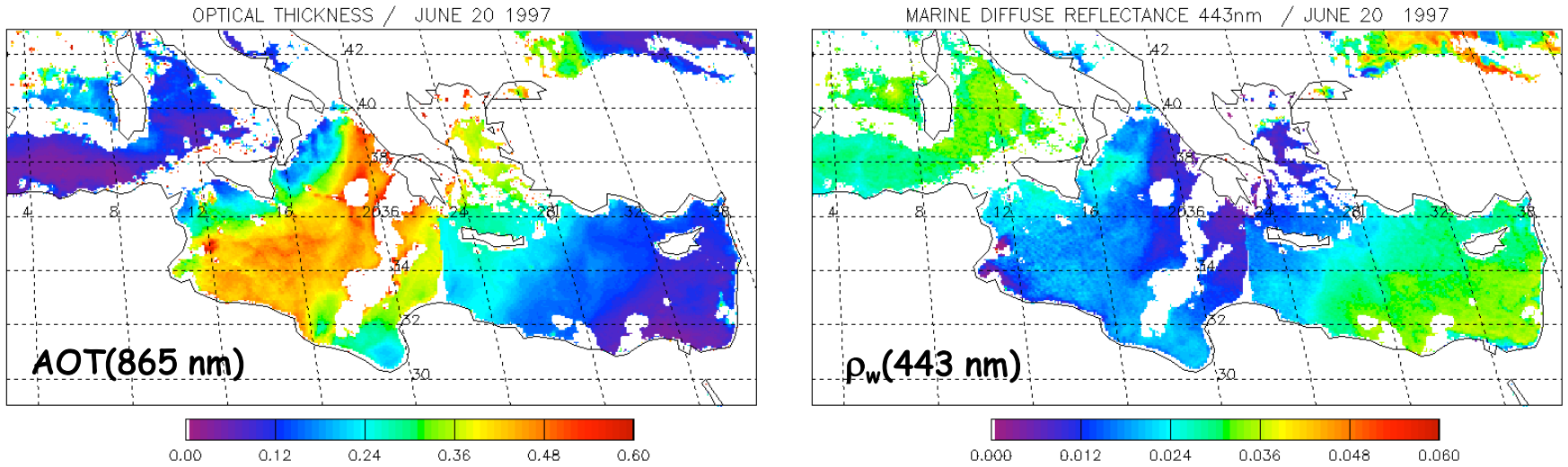

Figure 1-3: *Aerosol optical thickness (top) and marine reflectance (bottom) derived from POLDER data on 20 June 1997 using an atmospheric correction scheme that neglects aerosol absorption. The presence of a strong dust storm out of Libya to Greece results in a strong underestimation of the marine reflectance.*

-Standard atmospheric correction strongly underestimates ρ_w(443 nm).

How to deal with absorbing aerosols?

4) One may detect the presence of absorbing aerosols (e.g., by looking at the retrieved water reflectance at wavelengths where it is expected to be known and constant) and use more appropriate LUTs.

2) One may estimate individual aerosol properties, using various techniques, but accuracy may not be sufficient to perform suitable atmospheric correction.

3) One may use the entire information available (e.g., spectral observations from UV to SWIR):

-to estimate simultaneously the key properties of aerosols and water constituents by minimizing an error criterion between the measured reflectance and the output of a RT model.

-To cast atmospheric correction as a statistical inverse problem and to define a solution in a Bayesian context (e.g., estimating a function to perform from RT simulations a mapping from the TOA reflectance to the water reflectance).

4) One may exploit some properties of aerosol absorption on TOA reflectance (e.g., dependence on molecular scattering, therefore angular geometry).

SeaWiFS, Sea of Japan, 7 April 2001

RGB composite

S2001097031924_Lt_truecolor_AceAsia

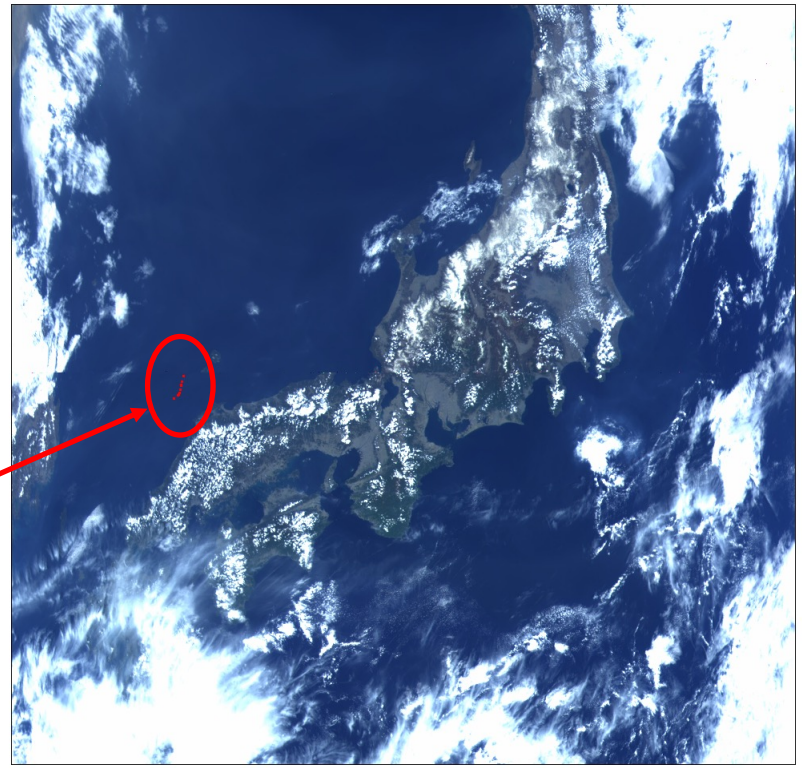

In-situ data

ρ_{TOA}(865 nm)

S2001097031924_Ref_865

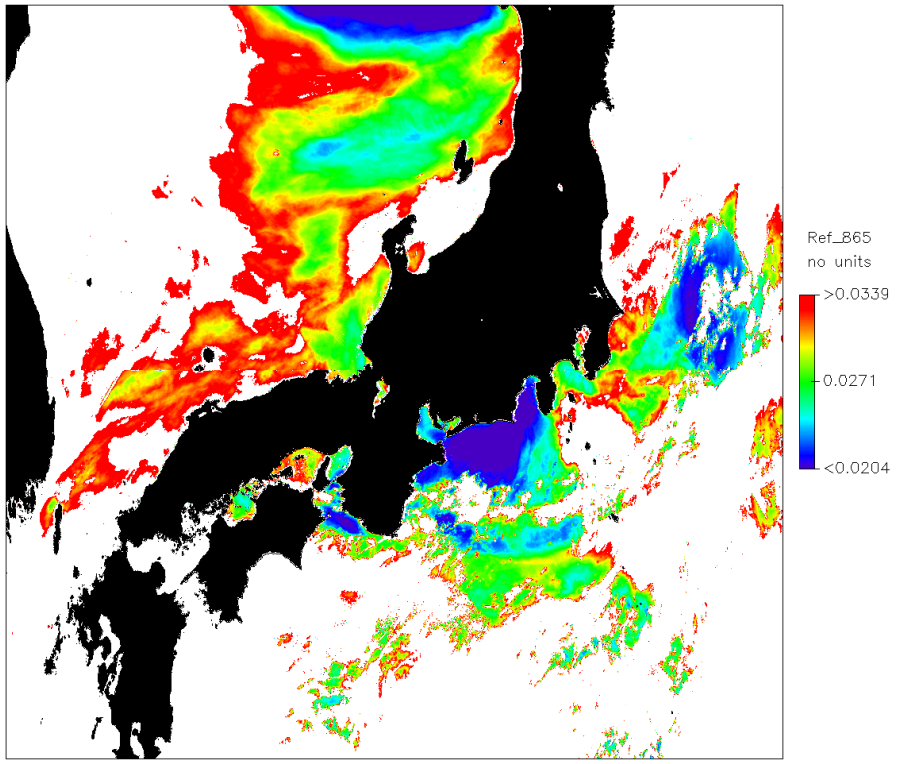

-Very polluted air and relatively stable and low (<500 m) MBL heights. 500 m trajectories from Japan, Korea, and Northern China.

***Figure 1-4**: SeaWiFS imagery of the Sea of Japan, 7 April 2001, showing location of in-situ measurements within ± 2 hours of satellite overpass (red dots). Left: RGB composite. Right: TOA reflectance at 865 nm.*

Bayesian vs. Standard AC, Sea of Japan, 7 April 2001

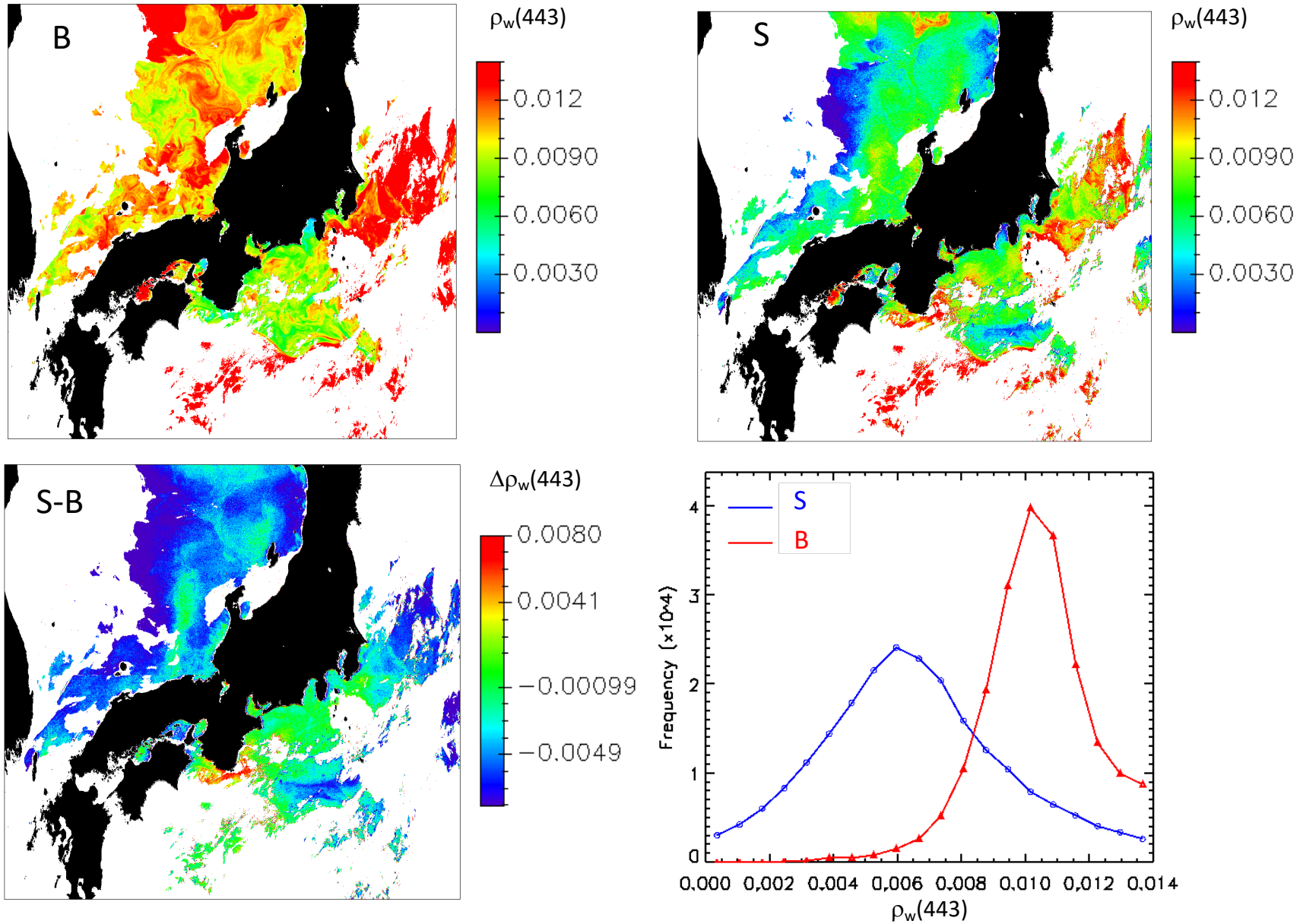

Figure 1-5: Estimated $\rho_w(443)$, Sea of Japan, 7 April 2001, in the presence of absorbing aerosols.

SeaWiFS, East China Sea, April 15, 2001

RGB composite

S2001105040514_Lt_truecolor_AceAsia

ρ_{TOA}(865 nm)

S2001105040514_Ref_865

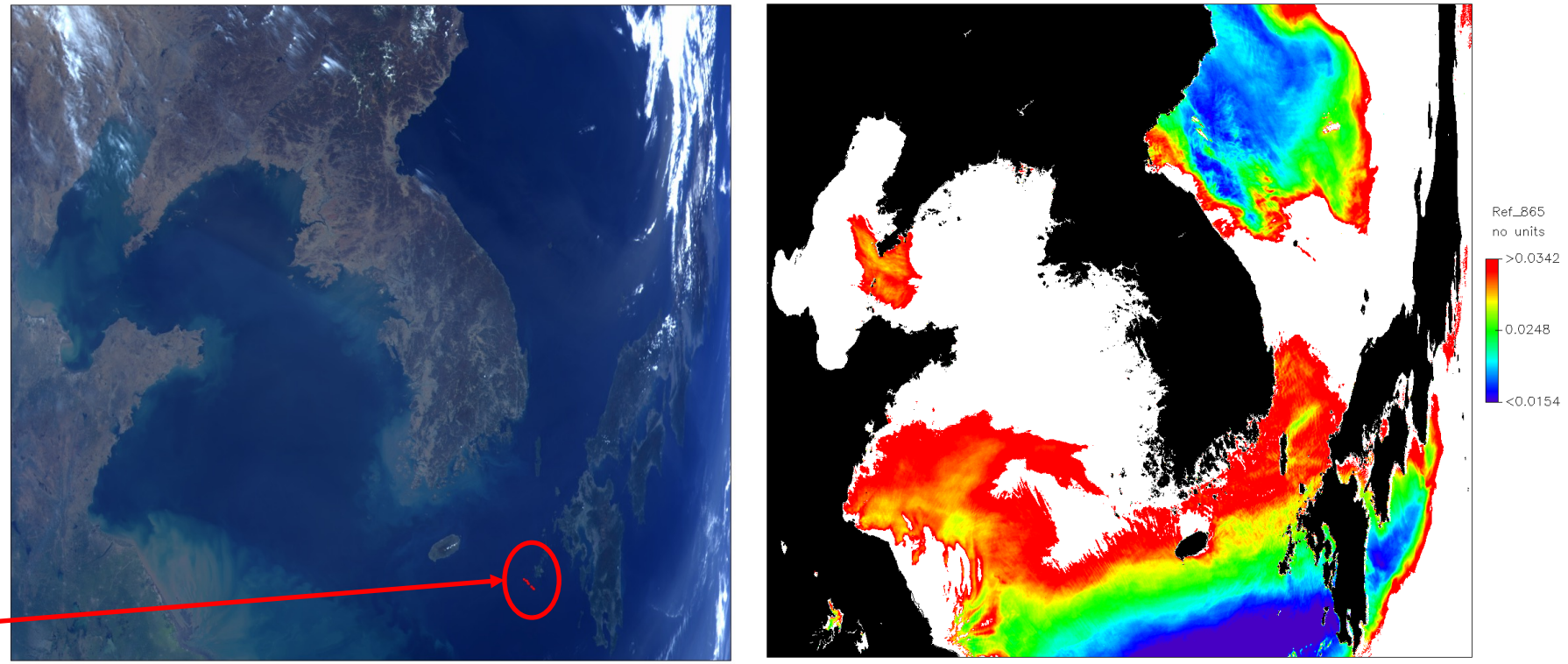

-Moderately polluted air and well-capped MBL with a height < 1 km. 500 m trajectories from Yellow Sea, Northeastern Mongolia, and Northern China.

***Figure 1-6**: SeaWiFS imagery of the East China Sea, 15 April 2001, showing location of in-situ measurements within ± 2 hours of satellite overpass (red dots). Left: RGB composite. Right: reflectance at 865 nm.*

Bayesian vs. Standard AC, East China Sea, April 15, 2001

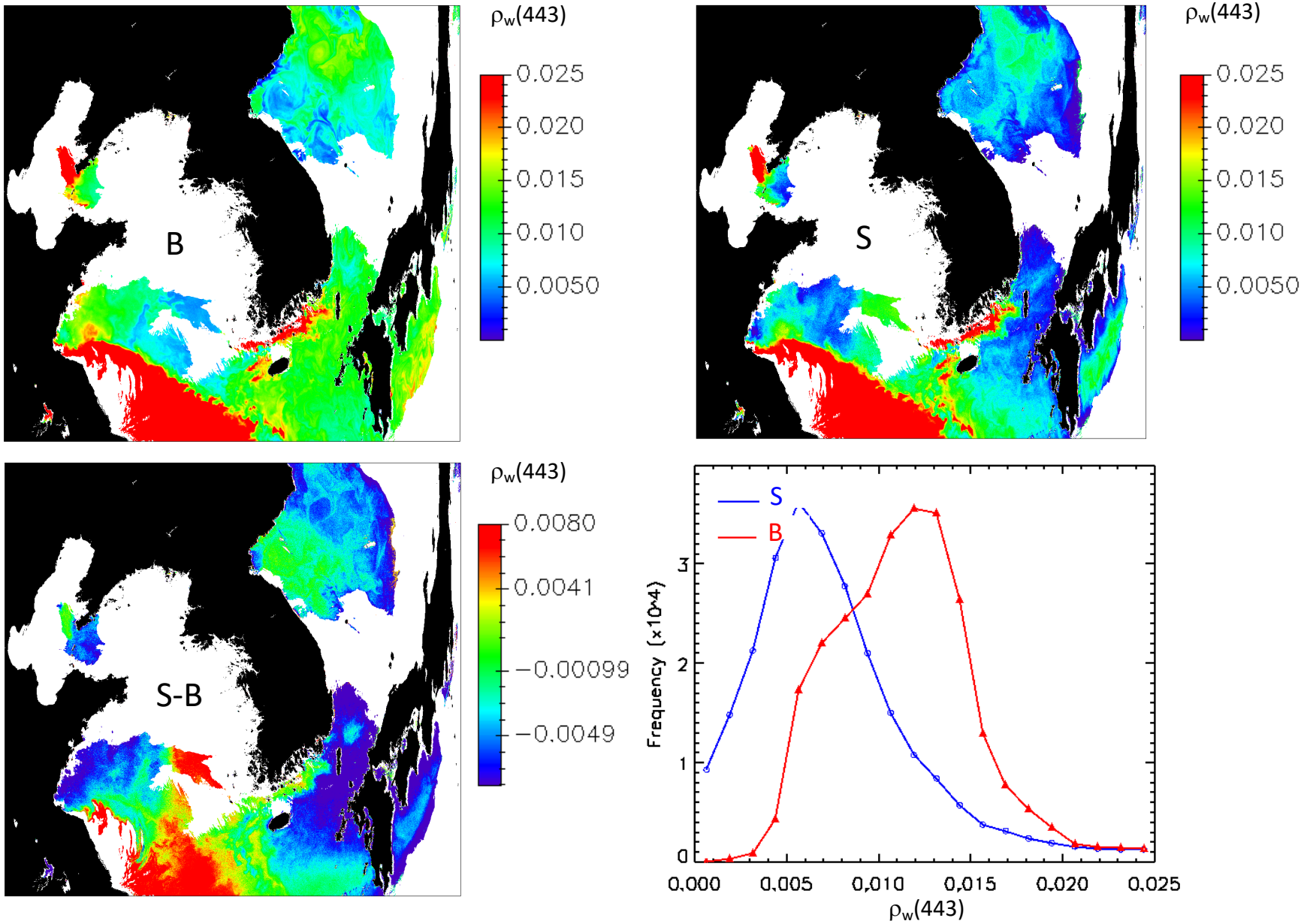

Figure 1-7: Estimated $\rho_w(443)$,East China Sea, April 15, 2001, in the presence of absorbing aerosols.

Evaluation against in-situ measurements: Bayesian versus Standard

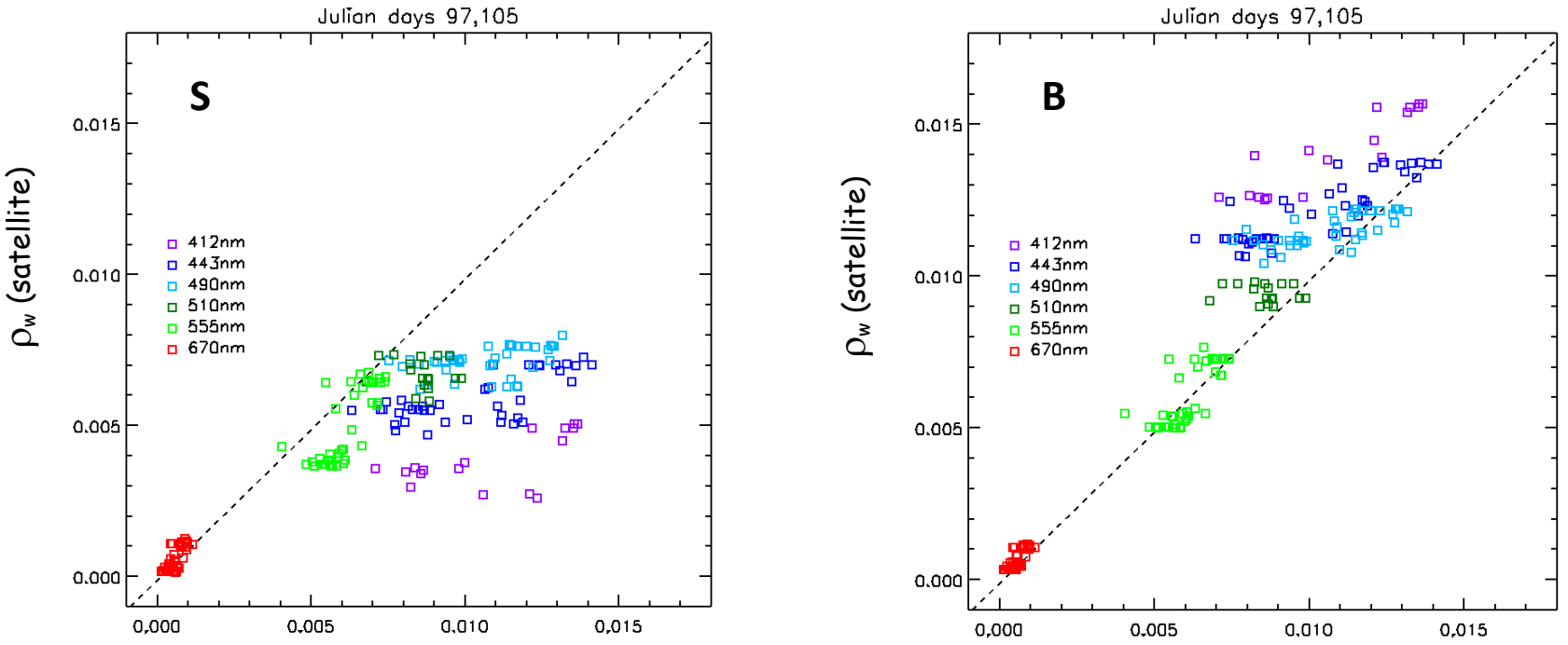

***Figure 1-8**: Comparison of satellite-derived marine reflectance with in-situ measurements, in the Sea of Japan and East China Sea, April 7 and 15, 2001. Left: Marine reflectance derived by the standard OBPG algorithm. Right: Marine reflectance derived by the statistical algorithm. The values in the blue are underestimated by the standard algorithm due to the presence of absorbing aerosols and overestimated by the statistical algorithm. The statistical values are in better agreement with the measurements.*

Using angular information

-After removing the atmospheric scattering effects, the TOA reflectance becomes approximately:

$$\rho_{TOA}' \approx \rho_{a\_abs} + T_a \rho_w$$

$$\rho_{TOA}' \approx -(P_s - P_{aer})/P_s \, \tau_{abs} m^* \rho_{mol} + \rho_w T_a (1 - \tau_{abs} m^*)$$

-By regressing ρ_{TOA}' versus $m^*\rho_{mol}$ (depends on geometry) one may get an estimate of the marine reflectance ρ_w. In practice, the problem is non-linear, and one my use different absorption predictors, such as the absorption effect for a typical aerosol.

-The aerosol variables that govern the absorption effect, i.e., absorption optical thickness and vertical distribution, do not need to be determined.

ρ_{TOA}'/T_{mol} versus $\rho_{mol}m^*$

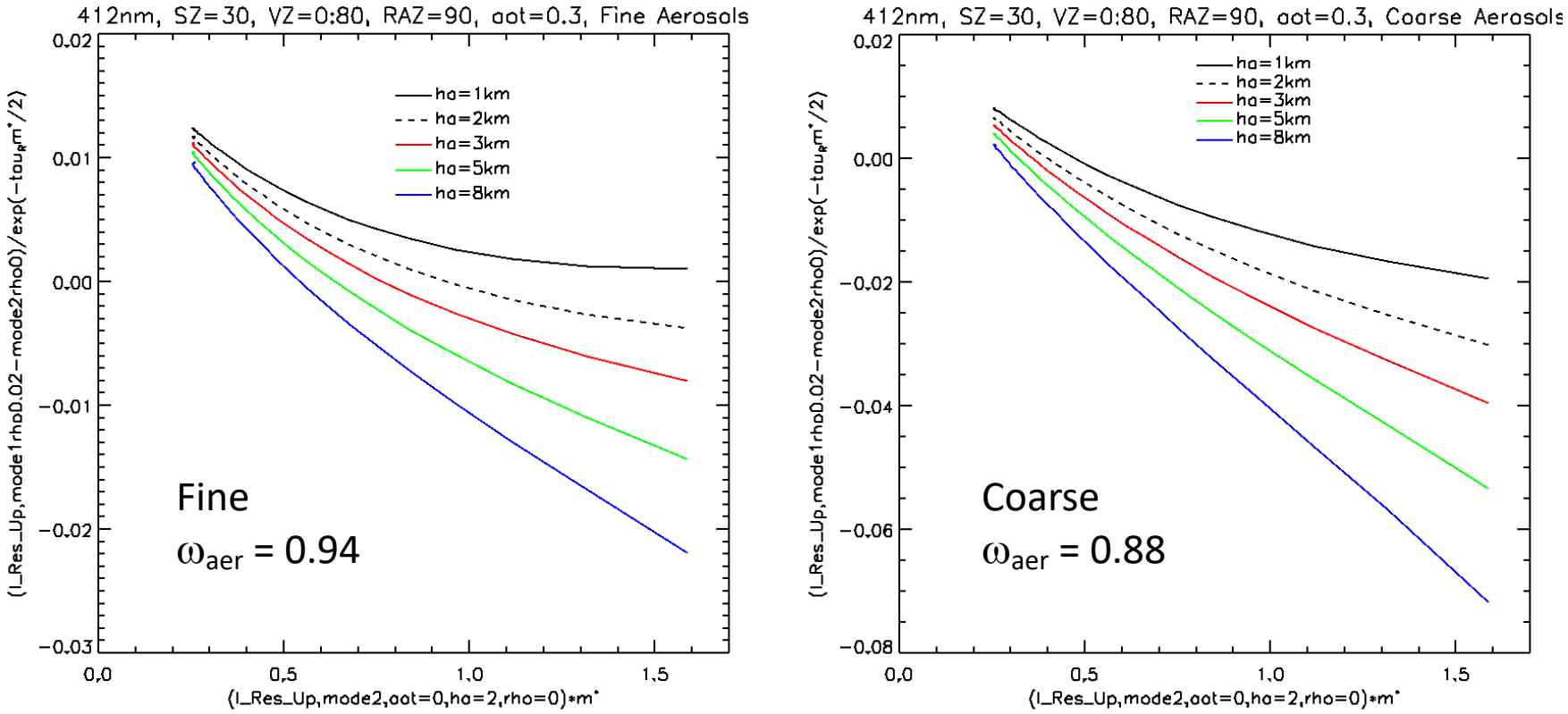

***Figure 1-9**: SOS simulations of ρ_{TOA}'/T_{mol} versus ρ_{mol} m* for fine aerosols (left) and coarse aerosols (right). Wavelength is 412 nm and aerosol optical thickness is 0.3. Wind speed is 5 m/s and marine reflectance is 0.02. Solar zenith angle is 30 deg., viewing azimuth angle varies between 0 and 80 deg., and relative azimuth angle is 90 deg. Aerosol scale height varies from 1 to 8 km (8 km correspond to mixed aerosols and molecules). The fine aerosols are defined by r_f = 0.1 µm , σ_f = 0.20, and m_f = 1.40 - 0.010i (single scattering albedo of 0.94), and the coarse aerosols by r_c = 2.0 µm , σ_c = 0.30, and m_c = 1.55 - 0.002i (single scattering albedo of 0.88).*

Theoretical performance of multi-angle AC, MISR

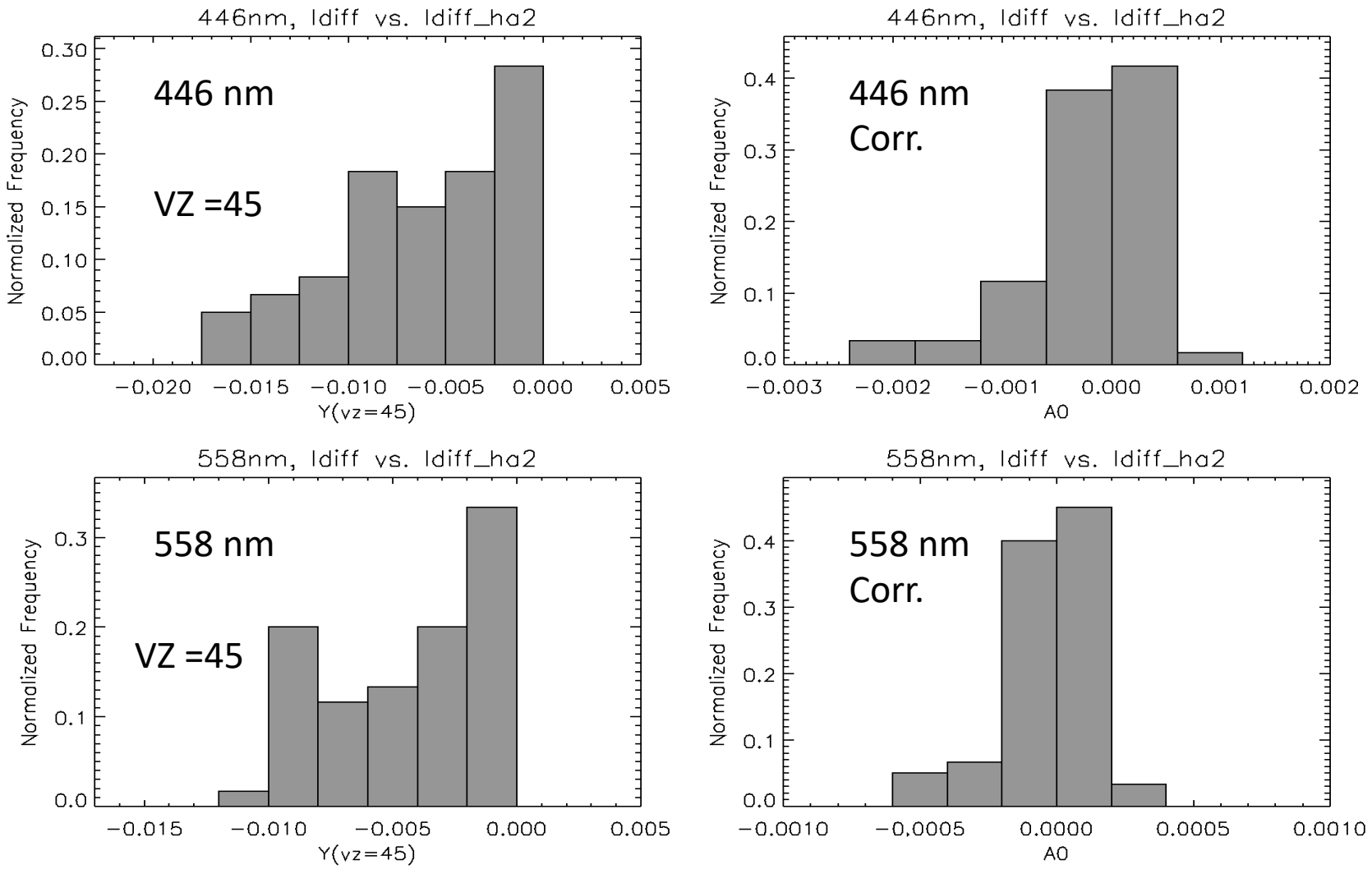

***Figure 1-10**: Expected Error on retrieved marine reflectance at 446 and 558 nm, before and after correction of the aerosol absorption effect. MISR viewing zenith angles of 26.1, 45.6, 60.0, and 70.5 deg. Various h_{aer} (1-8 km). τ_{aer} (0.1-0.5), absorbing aerosol types (fine, coarse), and SZ (30-60 deg.) are considered. RAZ = 90 deg.*

Application of multi-angle AC algorithm to POLDER imagery

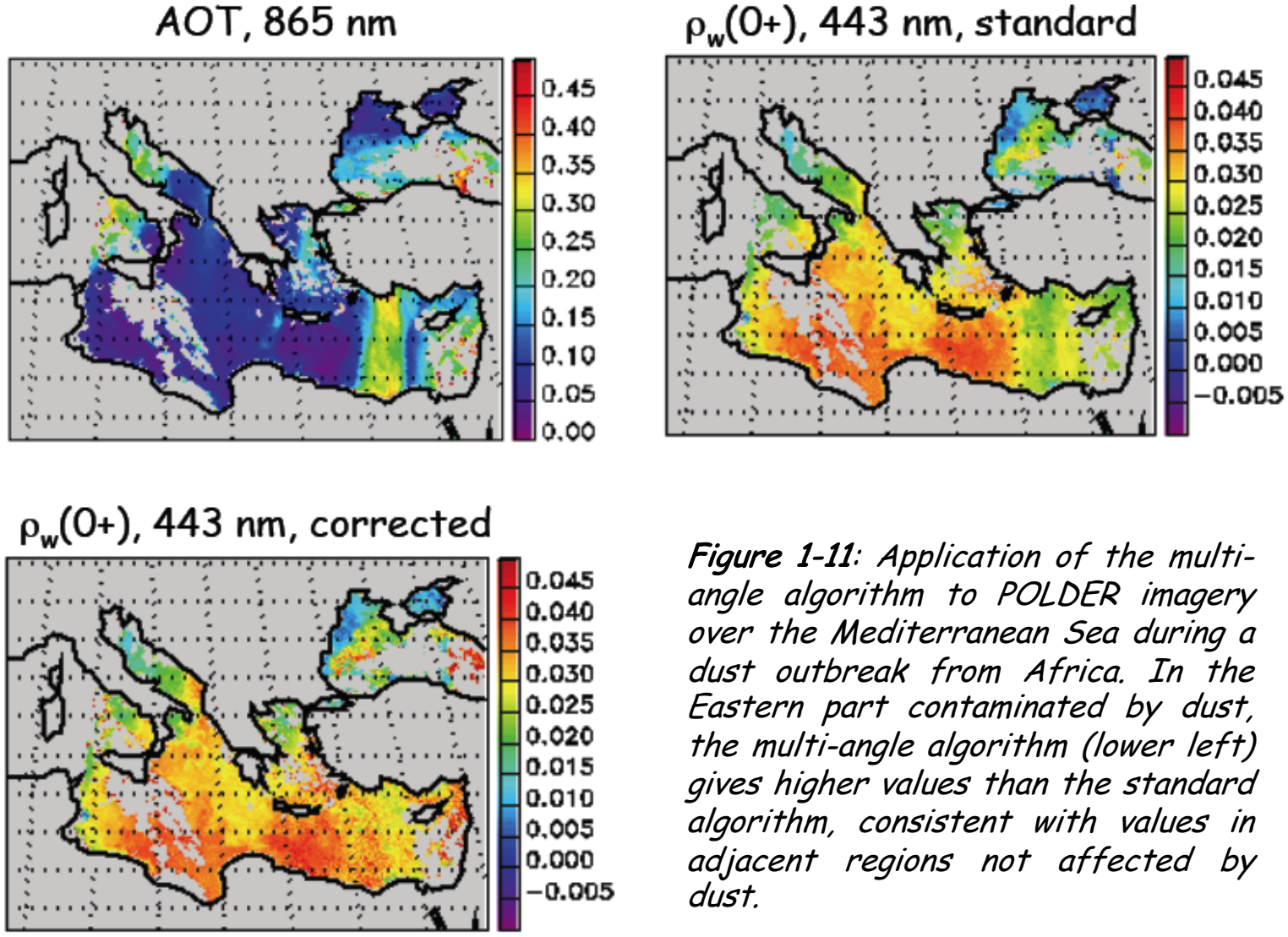

***Figure 1-11**: Application of the multi-angle algorithm to POLDER imagery over the Mediterranean Sea during a dust outbreak from Africa. In the Eastern part contaminated by dust, the multi-angle algorithm (lower left) gives higher values than the standard algorithm, consistent with values in adjacent regions not affected by dust.*

Conclusions about AC in the presence of absorbing aerosols

-Determining aerosol parameters separately may not be sufficiently accurate to compute aerosol reflectance and perform suitable correction. But aerosol retrievals may be used to constrain the solution in the standard algorithm.

-Including spectral observations in the visible, where the effect of absorbing aerosols is significant, may improve the AC of ocean-color imagery in the presence of absorbing aerosols. Further improvements are expected by observing in the UV, where the effect of absorbing aerosols is larger (OCI/PACE).

-Multi-angular information may be used to estimate directly the effect of aerosol absorption on the TOA reflectance. (The aerosol variables that govern the absorption effect, i.e., absorption optical thickness and vertical distribution, do not need to be determined.)

2. Whitecaps

Introduction

-When ocean waves break, they generate whitecaps, a mixture of air and water.

-Whitecaps may enhance dramatically the intensity and properties of sunlight diffusely reflected by the surface on temporal scales of seconds to minutes; They affect large areas such as the windy Southern Oceans.

-The enhanced reflectance from whitecaps, i.e., $A\rho_{wc}$ (product of fractional area A and reflectance ρ_{wc}), needs to be removed in order to produce water reflectance estimates suitable for standard ocean-optics applications.

-From space, since whitecap reflectivity is high, even a small amount of whitecap may be problematic for the retrieval of water reflectance.

-Whitecap properties (i.e., fractional area coverage, spectral reflectance) are extremely variable and, therefore, difficult to model with enough accuracy, a major challenge in ocean color remote sensing from space.

Seas with whitecaps

***Figure 2.1**: Examples of seas with whitecaps, showing various stages of wave breaking with surface foam, streaks, and under-water bubble plumes. The presence of whitecaps changes dramatically the aspect of the surface and its brightness.*

Measured ocean surface reflectance, with and without whitecaps

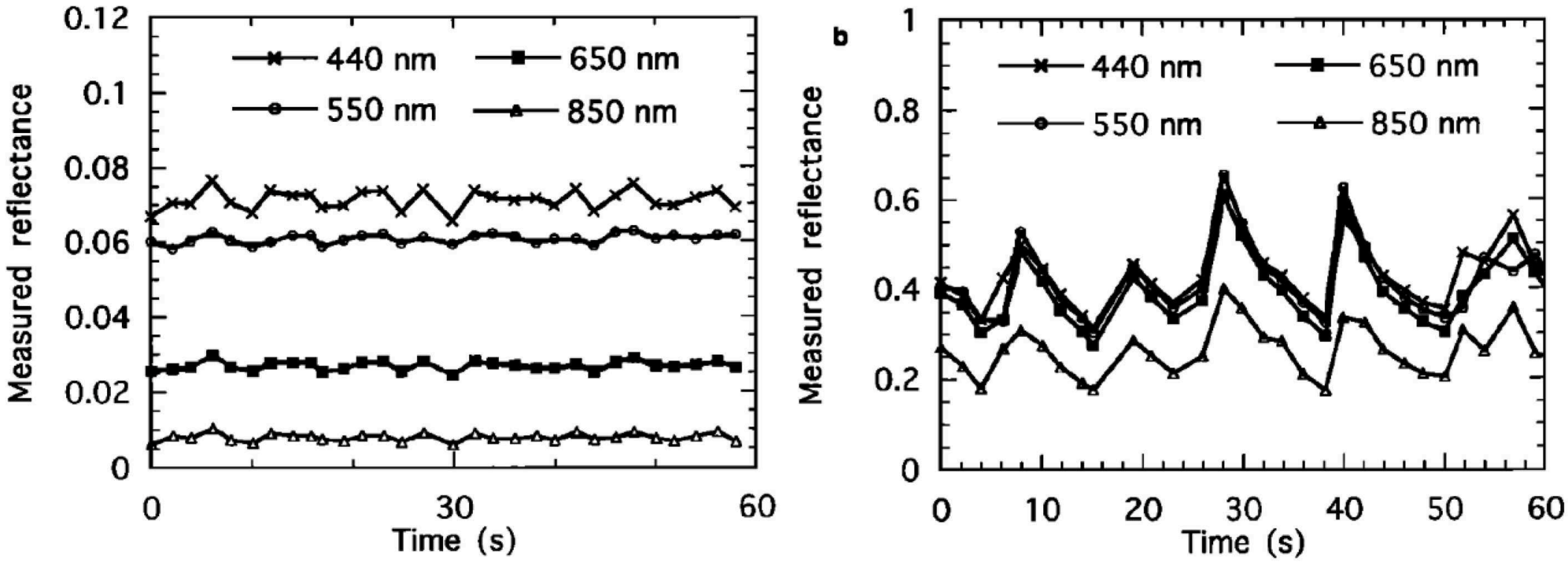

***Figure 2.2**: Time series of measured surface reflectance at 440, 550, 650, and 850 nm in the surf zone, in the absence and presence of breaking waves, left and right, respectively. When waves break, air is trapped and injected below the surface, creating surface foam and underwater bubble plumes, increasing substantially surface reflectance. (After Frouin et al., 1996.)*

Variability of whitecap spectral reflectance and fractional coverage

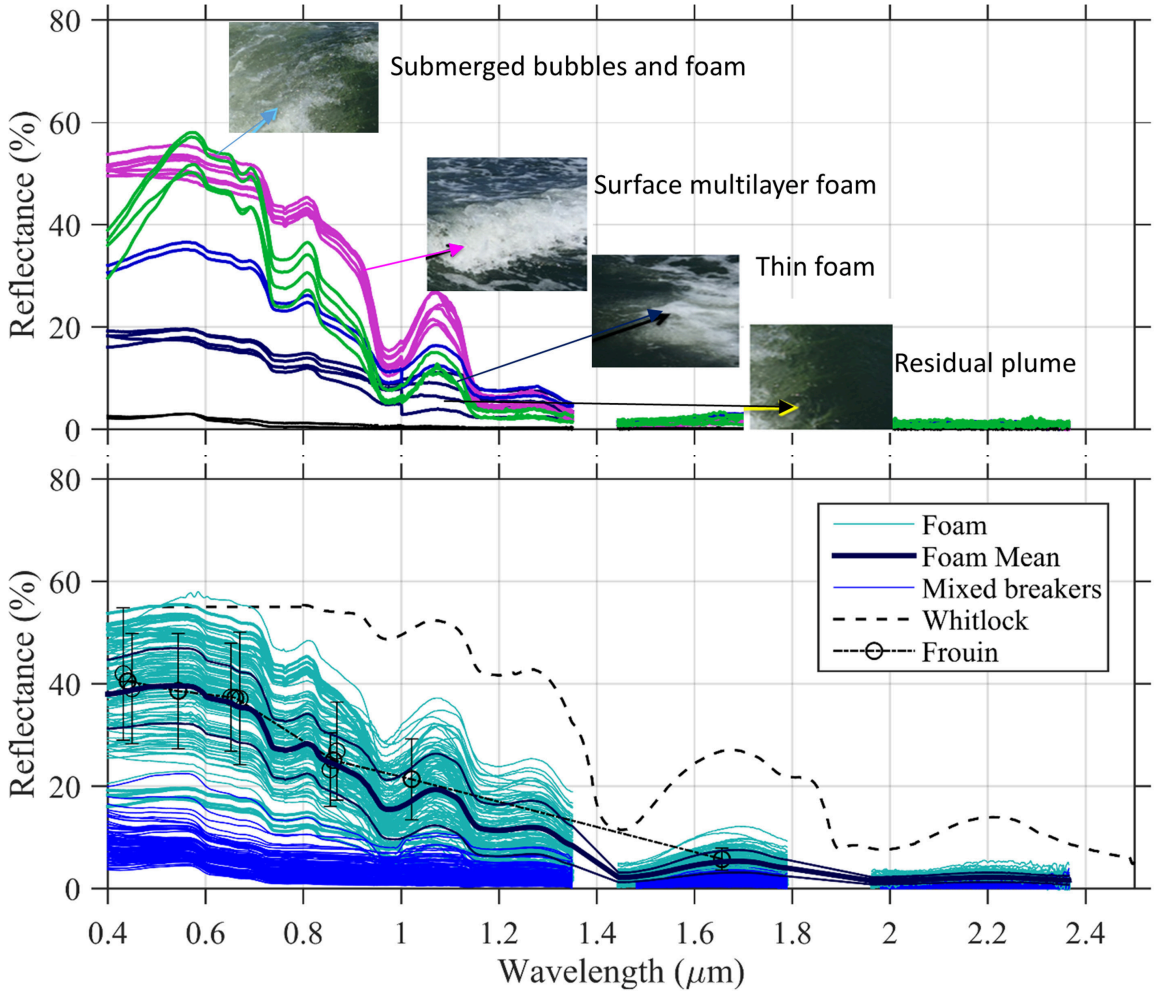

Figure 2.3: Top: Examples of manufactured whitecap reflectance and associated pictures of the sea surface. Bottom: Reflectance measured in Long Island Sound, USA of intense wave breaking from a ship bow (cyan) and mixed pixels of natural waves breaking (blue) in relationship to published studies. (After Dierssen, 2019.)

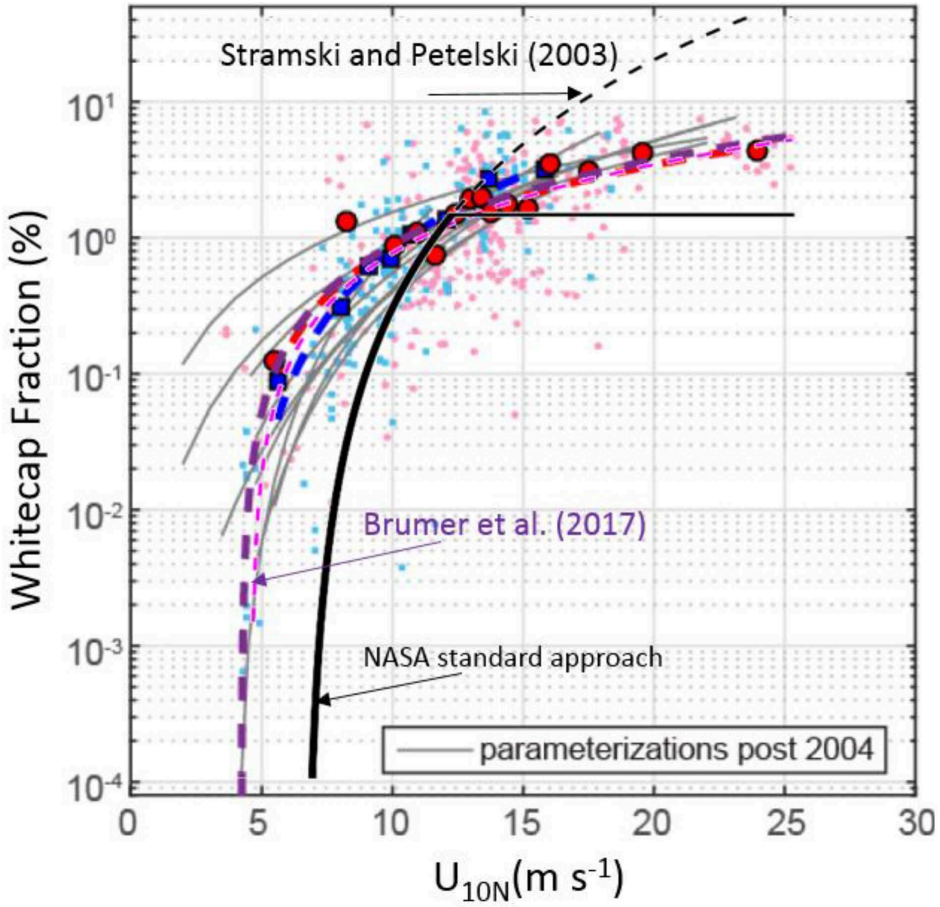

Figure 2.4: Measurements of "equivalent neutral" wind speed at 10 m and whitecap fraction from Southern Ocean Gas Exchange (blue) and HiWings (red) campaigns. Larger dots represent data binned over wind speed ranges and the dotted red line represents the mean from both campaigns. Thick black curve is the relation based on Stramska and Petelski (2003) used by NASA in the standard AC algorithm. (Adapted from Brumer et al., 2017.)

Impact on ocean color remote sensing: Error on water reflectance at 443 nm for different combinations of aerosol and whitecap reflectance

$$\rho_{TOA}/t_g \approx \rho_w + \rho_a + \rho_m + \rho_{wc}$$

***Table 2.1**: Error on water reflectance at 443 nm for several combinations of ρ_a and ρ_{wc} and some values of the Angstrom exponent α. $\rho_a + \rho_{wc}$ is fixed at 0.02. In the absence of whitecaps, the value of 0.02, i.e., ρ_a at 865 nm corresponds to typical aerosols having an optical thickness of 0.2 and observations at scattering angles of 90-120 deg. A positive value of the error corresponds to an overestimation of the correction or an underestimation of the marine reflectance. (After Frouin et al., 1996.)*

Whitecaps behave as gray bodies

	α			
$\rho_{wc}/(\rho_a + \rho_{wc})$	0	0.5	1.0	1.5
0	0	0	0	0
0.5	0	-0.0002	-0.0010	-0.0026
1	0	0	0	0

Whitecap reflectance varies spectrally

	α			
$\rho_{wc}/(\rho_a + \rho_{wc})$	0	0.5	1.0	1.5
0	0	0	0	0
0.5	0.0158	0.0178	0.0195	0.0209
1	0.0429	0.0429	0.0429	0.0429

-Using the gray model, the extrapolation scheme introduces small errors, except when Angstrom exponent is above 1.

-Using the spectrally dependent model, errors become catastrophic as soon as there is even a small amount of whitecap, mixed or not with aerosols, thus irrespective of aerosol type.

Whitecap Reflectance Modeling

-When waves break, they generate surface foam (air cavities separated by thin water layers) and underwater bubbles. These bubbles increase photon path in the water, i.e., enhance absorption effects.

-To capture these essential physics, one can model whitecaps as a 2-layer system, each layer having a different spectral behavior:

a) A semi-transparent foam layer at the surface of reflectance ρ_f, characterized par its value at a reference wavelength (e.g., 400 nm), ρ_{f0}, and its spectral dependence (Whitlock et al., 1982), $f(\lambda)$, i.e., $\rho_f = \rho_{f0} f(\lambda)$;

b) A bubble layer below of reflectance ρ_b, characterized by its geometrical thickness, H_b, and its optical thickness, τ_b.

-The total whitecap reflectance, ρ_{wc}, is then expressed as:

$$\rho_{wc}(\rho_{f0}, H_b, \tau_b) = \rho_{f0} f + \rho_b(H_b, \tau_b) (1 - \rho_{f0} f)^2 / [1 - \rho_b(H_b, \tau_b) \rho_{f0} f]$$

Phase function for underwater bubble layer

-Bubble probability density follows Junge power law with -4 exponent according to Kolovayev (1988), Johnson and Cooke (1979, and Baldy (1993):

$f(r) = f_0$ for $10<r<50$ mm;

$f(r) = f_0(r/50)^{-4}$ for $50<r<500$ mm

where r is bubble radius and f_0 is defined by $(\int f(r)dr)=1$.

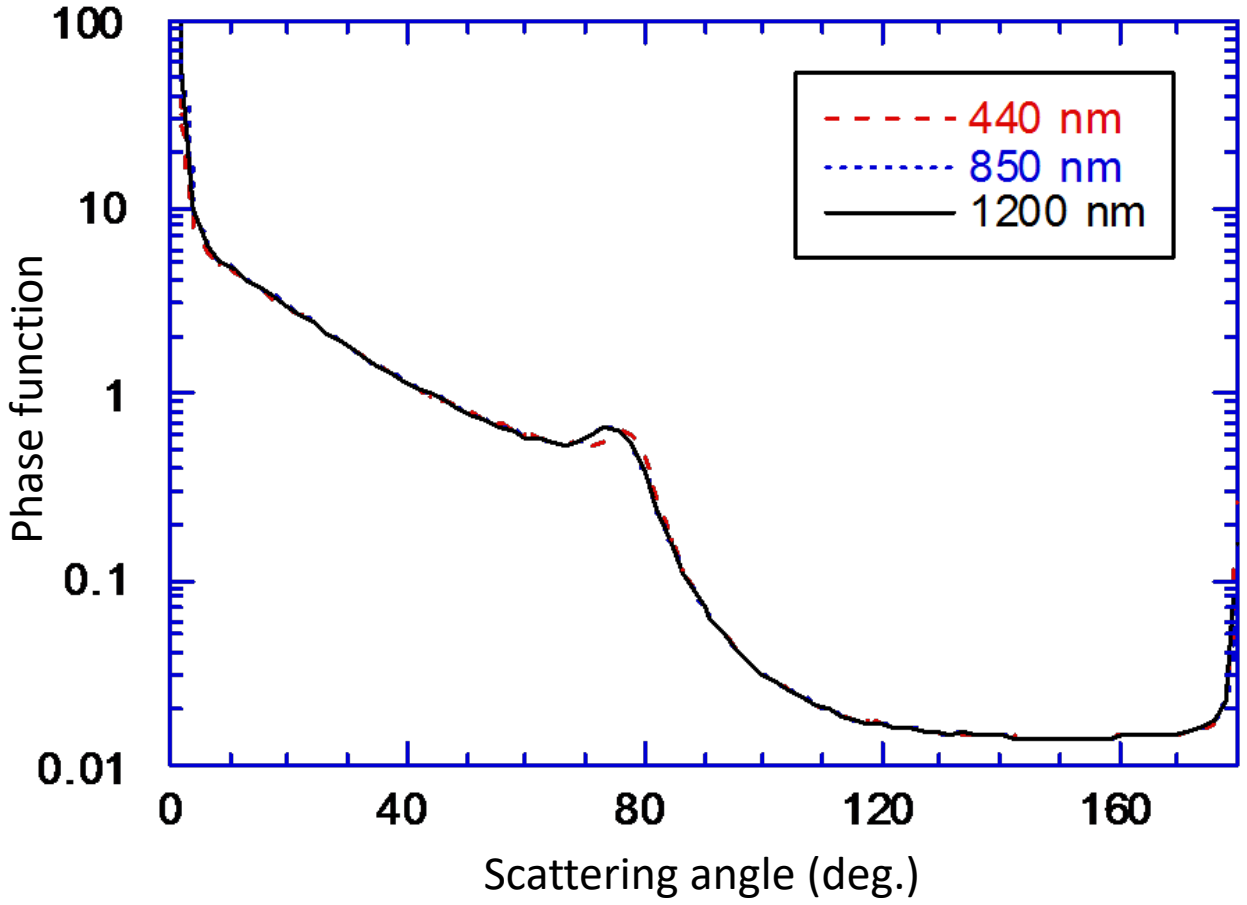

Figure 2.5: Phase function of air bubbles in water for wavelengths of 440, 850, and 1200 nm, calculated using Mie theory and bubble size spectra of Baldy (1987). Critical angle is 82.5 deg.

Reflectance of underwater bubble layer

- ρ_b calculated approximately as the sum of normalized contributions of radiances at each order of scattering n, L_n, weighted by the probability to be scattered at this order, ω_0^n, i.e.,

$$\rho_b(\theta_s, \theta_v, \phi) \approx 1/\cos\theta_s \sum_n [\omega_0^n L_n(\theta_s, \theta_v, \phi)] \text{ with } \omega_0 = \tau_b/(\tau_b + a_w H_b)$$

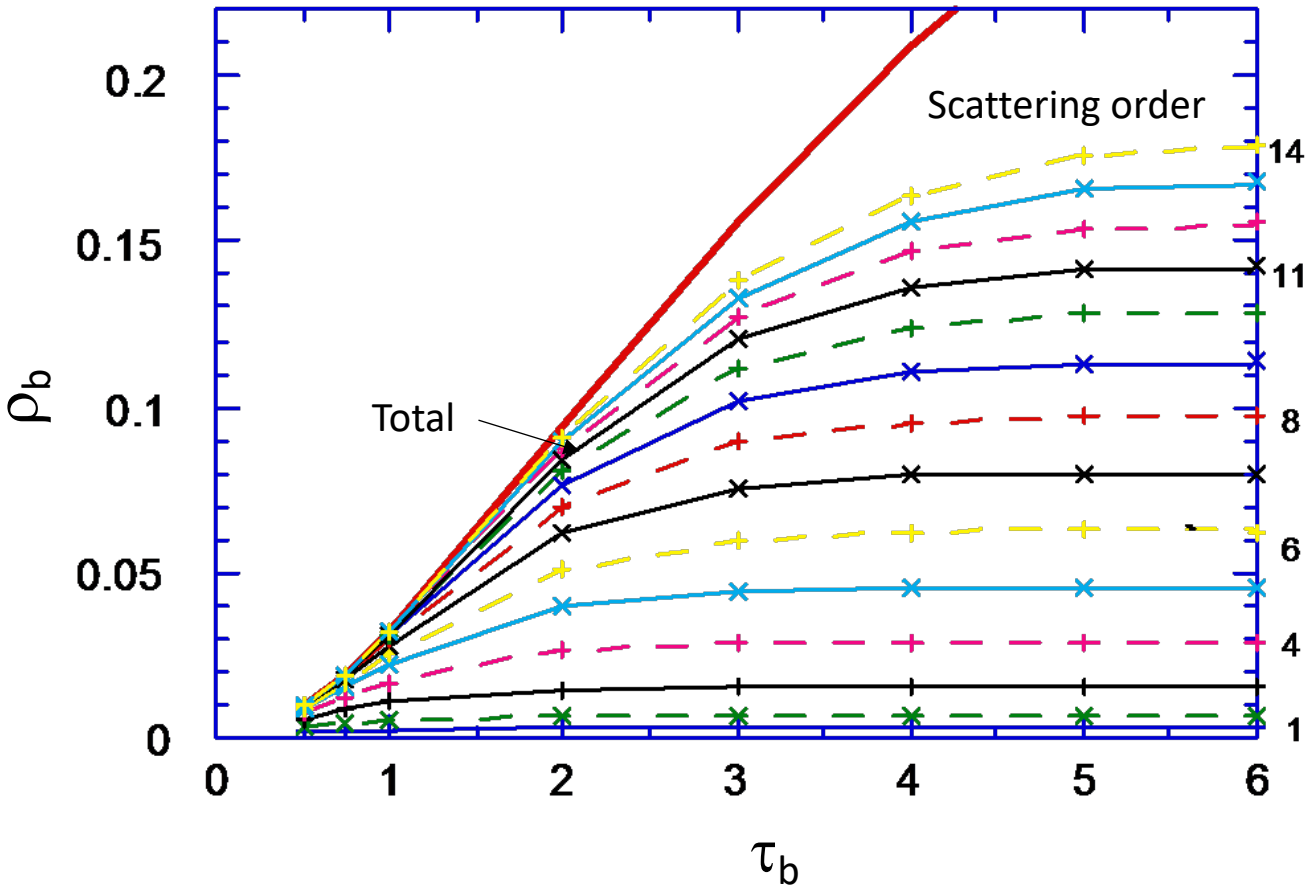

Figure 2.6: Contribution of various scattering orders to ρ_b. Single scattering albedo is unity, Sun zenith angle s 45 deg., and backscattering viewing.

Bubble layer is a very scattering medium:

1) Single scattering plays little role (<5% for τ_b>2.

2) The average number of scattering events by a photon is large (>14 for τ_b>3).

Simulations and application to in-situ measurements

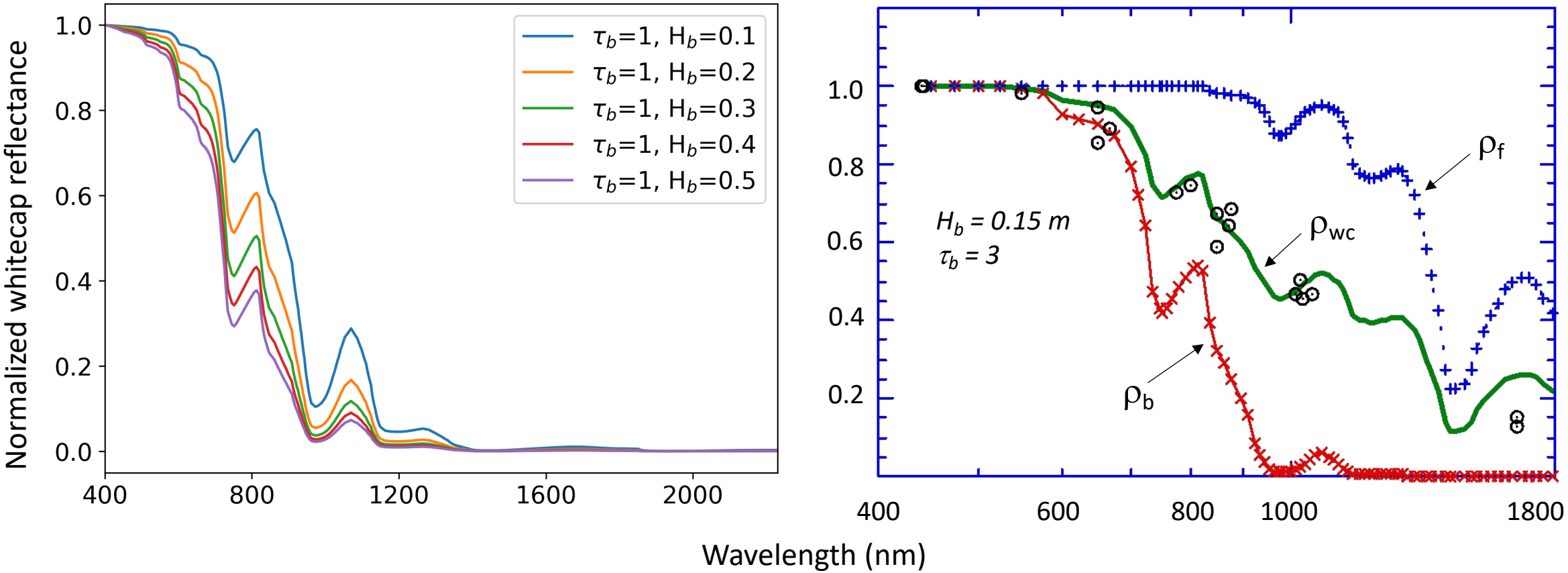

***Figure 2.7**: Left: Simulations of spectral dependence of whitecap reflectance for an underwater bubble layer of variable geometric thickness (0.1, 0.2, 0.3, 0.4, and 0.5 m and optical thickness of 1. Sun zenith angle is 30 deg. and viewing is in backscattering. Absorption effects increase as H_b increases. Right: Comparison between normalized surface foam reflectance (blue), underwater bubble reflectance for H_b = 0.15 m and τ_b of 3 (red), the resulting whitecap reflectance (green), an in-situ measurements collected at the Scripps Institution of oceanography Pier in 1994 and 1995.*

Inversion using PACE OCI wavelengths in NIR and SWIR, no atmosphere

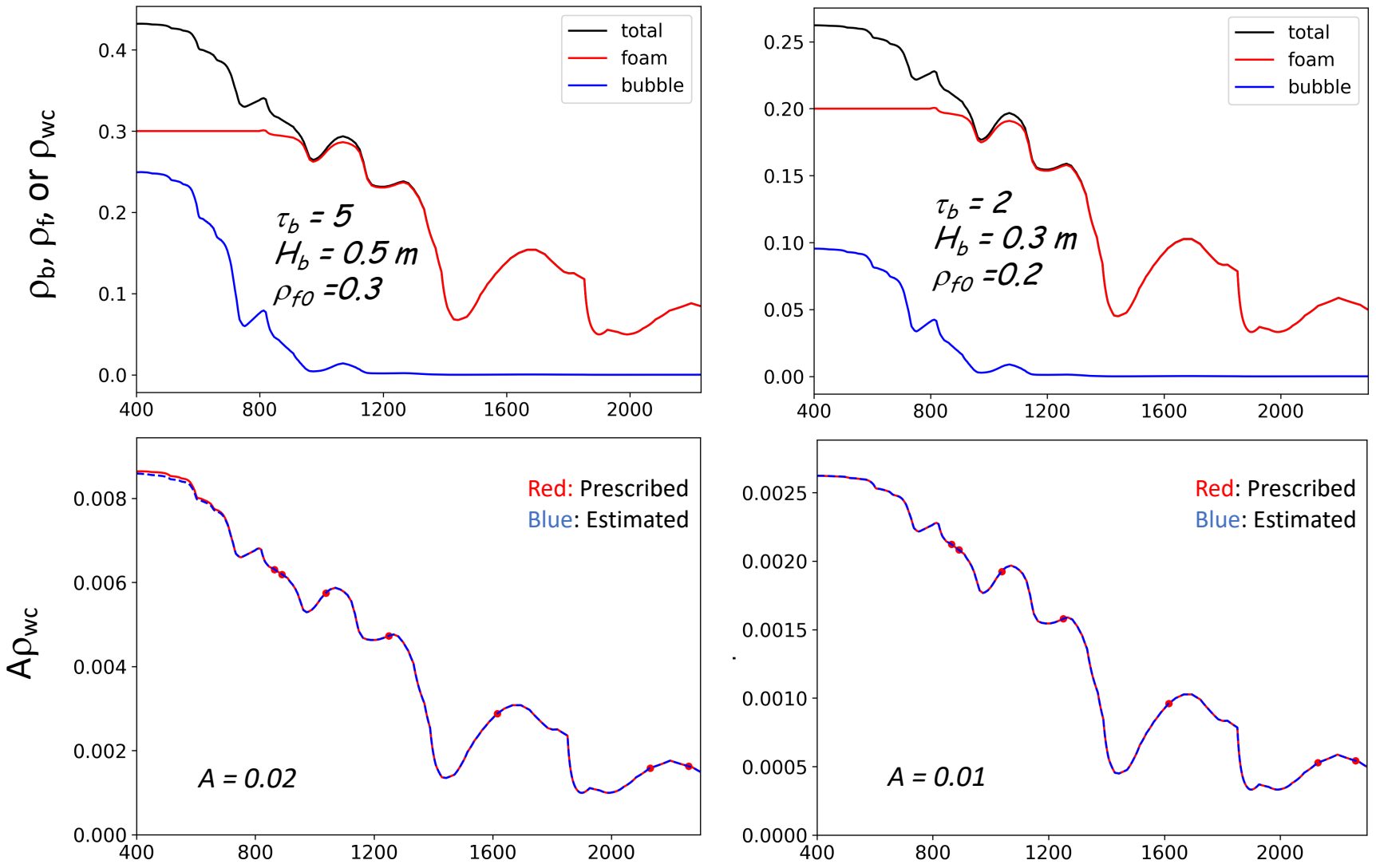

-Spectral bands: 865, 890, 1038, 1250, 1615, 2130, and 2250 nm.

-Nelder/Mead optimization.

-Model parameters are well retrieved, allowing accurate $A\rho_{wc}$ estimates in the entire spectral range.

Top: Prescribed ρ_{wc} (Case 1, left: τ_b = 5, H_b = 0.5 m, ρ_{f0} =0.3; Case 2, right: τ_β = 2, H_b = 0.3 m, ρ_{f0} =0.2). Bottom: retrieved and prescribed $A\rho_{wc}$ for Case 1 with A = 0.02 and case 2 with A = 0.01.

Inversions, no atmosphere, for varied values of A, ρ_{f0}, H_b, and τ_b

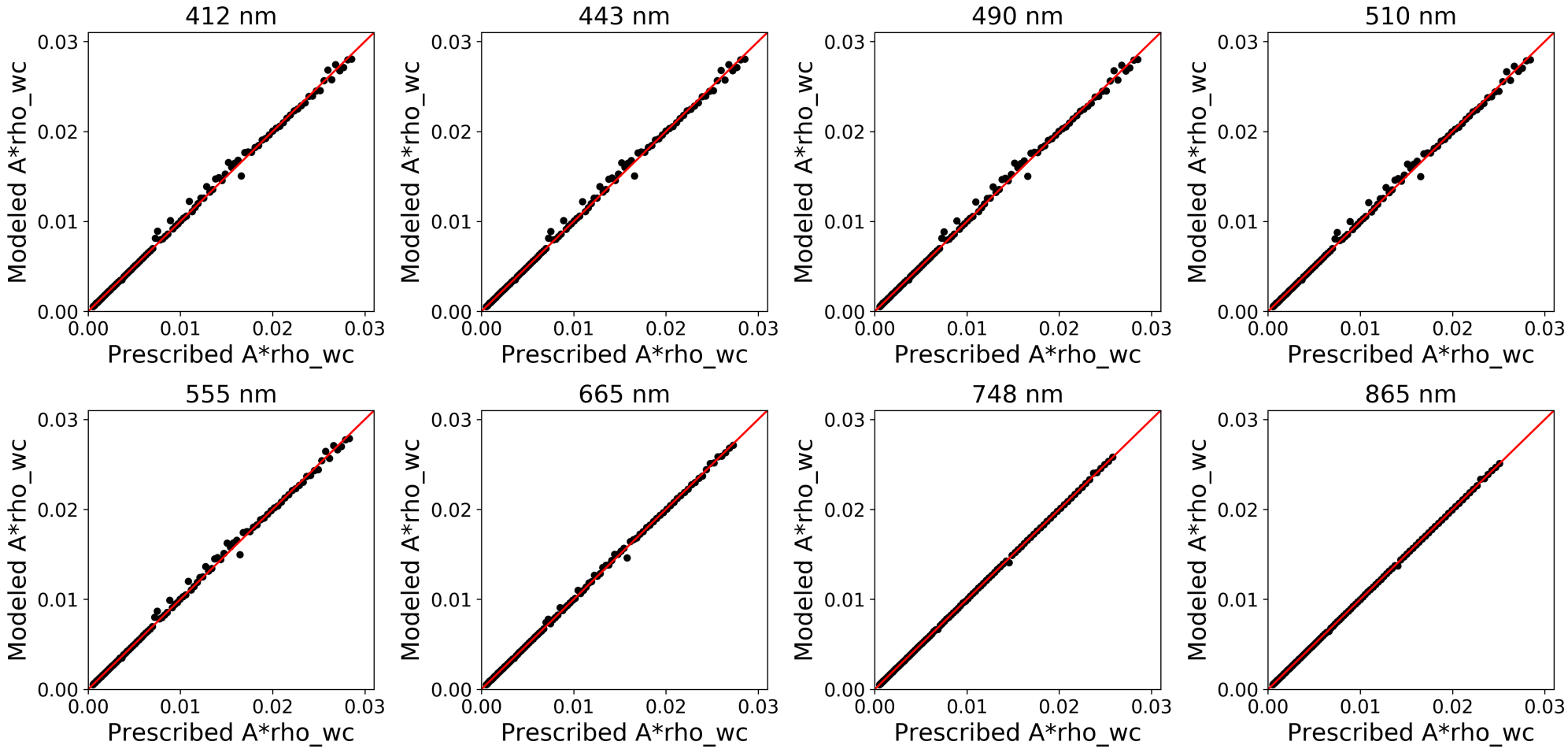

Figure 2.8: Modeled versus prescribed Ar_{wc} for 100 cases with A, ρ_{f0}, H_b, and τ_b values randomly selected in the ranges 0.01 to 0.1, 0.1 to 0.5, 0.1 to 0.5 m, and 0.5 to 5, respectively. Inversion (in the absence of noise) is robust using the PACE OCI spectral bands in the NIR and SWIR, allowing reconstruction of whitecap signal at short wavelengths.

Inversion from top-of-atmosphere

-Inversion from TOA using PACE OCI spectral bands in NIR/SWIR (only 7 usable bands) is ill-conditioned, because atmospheric parameters also need to be retrieved. Additional spectral bands are necessary.

-Spectral dependence of ρ_{wc} can be expressed as a function of ω_0, allowing ρ_{wc} to be modeled as a weighted combination of 2 extreme cases, the case of the surface foam and a case of underwater bubbles, i.e., the number of parameters characterizing ρ_{wc} is reduced from 3 to 2:

$$\rho_{wc} = \rho_{wc0}\{P[\alpha_f/(\alpha_f + a_w)] + (1 - P)\,[\alpha_b/(\alpha_b + a_w)]\}$$

P: mixing parameter (0-1); ρ_{wc0}: whitecap reflectance at a reference wavelength; α_f and α_b: pre-determined coefficients.

-Signal of atmosphere + surface may be sufficiently smooth spectrally to be modeled with a few parameters, if wavelengths are properly selected.

Conclusions about AC in the presence of whitecaps

-From space, since whitecap reflectivity is high, even a small fraction of whitecaps within the instrument's elementary field of view (i.e., within a pixel) may be problematic, which may lead to water reflectance errors much larger (i.e., by an order of magnitude) than the requirements.

-Whitecap reflectance can be modeled reasonably well by assuming whitecaps as a two-layer system, with foam at the surface and entrained bubbles below.

-The two layers have spectrally different behaviors, the underwater bubble layer enhancing absorption. The model depends on 3 parameters, i.e., ρ_{f0}, H_b, and τ_b.

-The model allows a good representation of in situ measurements of whitecap reflectance, especially its spectral dependence, a key parameter in ocean color remote sensing.

Conclusions about AC in the presence of whitecaps (cont.)

-In the absence of atmosphere, the whitecap spectral signal, i.e., $A\rho_{wc}$ can be retrieved accurately from measurements at the PACE OCI wavelengths in the NIR and SWIR, but inversion from TOA measurements is ill-conditioned. Additional spectral bands in the NIR and SWIR are necessary for robust inference.

-For PACE, using standard AC algorithm, one may still have to rely on some assumptions about optical properties of whitecaps and their fractional coverage (one may not be able to estimate them directly from the available measurements).

-AC algorithms robust to whitecaps, in which the perturbing signal to correct is modeled to implicitly include the whitecap signal (e.g., POLYMER-type), should be further explored.

3. Adjacency effects

Introduction

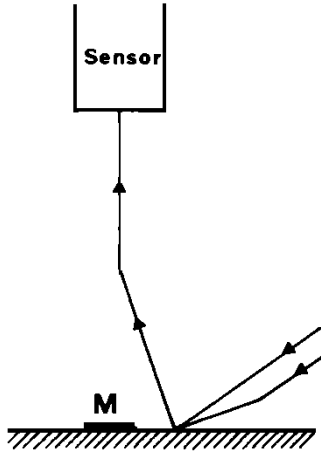

-Adjacency effects are caused by atmospheric scattering of radiance that originates outside of the sensor element's field of view.

-They are especially important in the the vicinity of land, clouds, and sea ice, i.e., when the spatial contrast between the target and its environment is relatively large.

-They may affect significantly the retrieval of water reflectance and derived products (e.g., chlorophyll concentration) at distances of 10-20 km.

-Adjacency effects are generally ignored in standard atmospheric correction schemes and operational processing of satellite ocean-color imagery.

Example of Adjacency effect

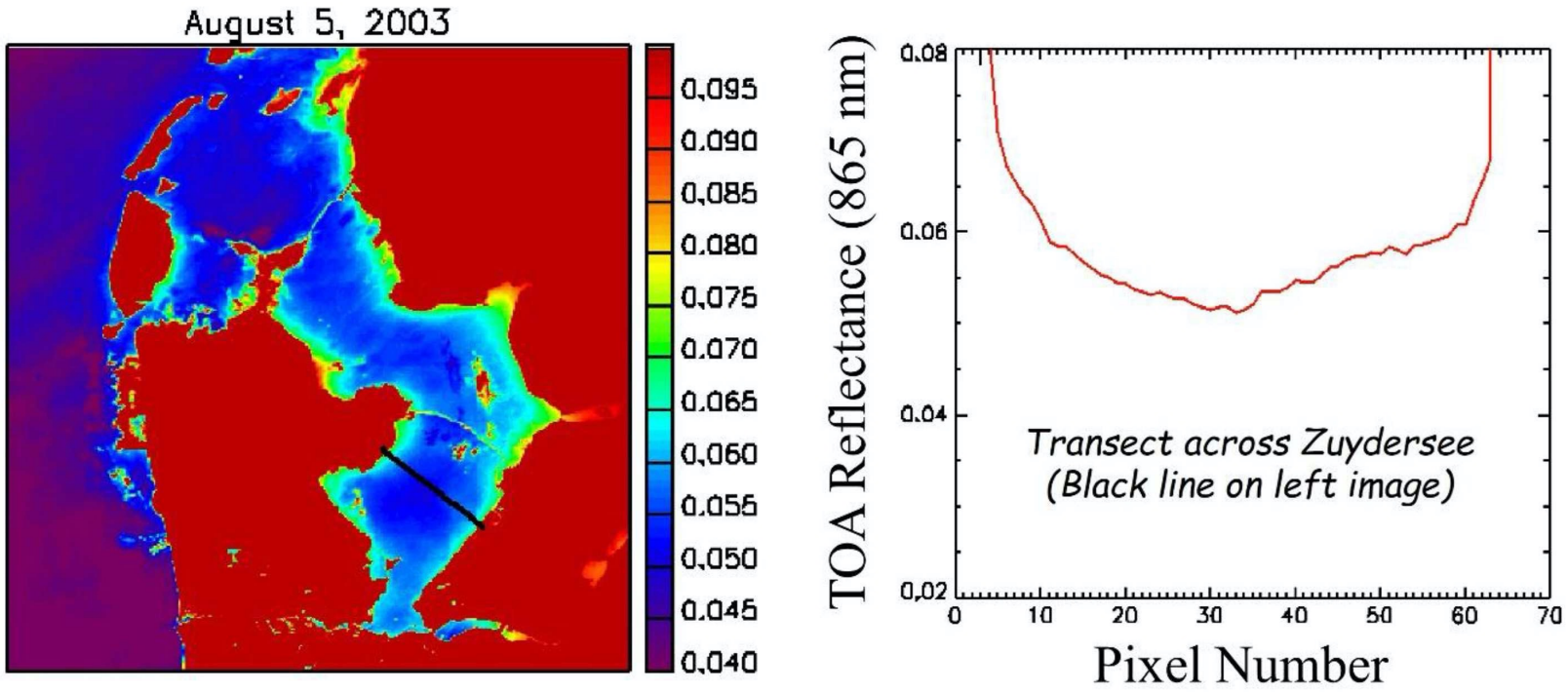

***Figure 3.1**: Left: Image of TOA reflectance at 865 nm acquired by MERIS (1 km resolution) over the Netherlands on 5 August 2003. Right: Reflectance along the black line in the image.*

-The measured signal over the Zuydersee is enhanced by reflected light from vegetated areas surrounding the target pixel (band of higher TOA reflectance values within 5–10 km of the coast).

RT simulations of the TOA adjacency effect

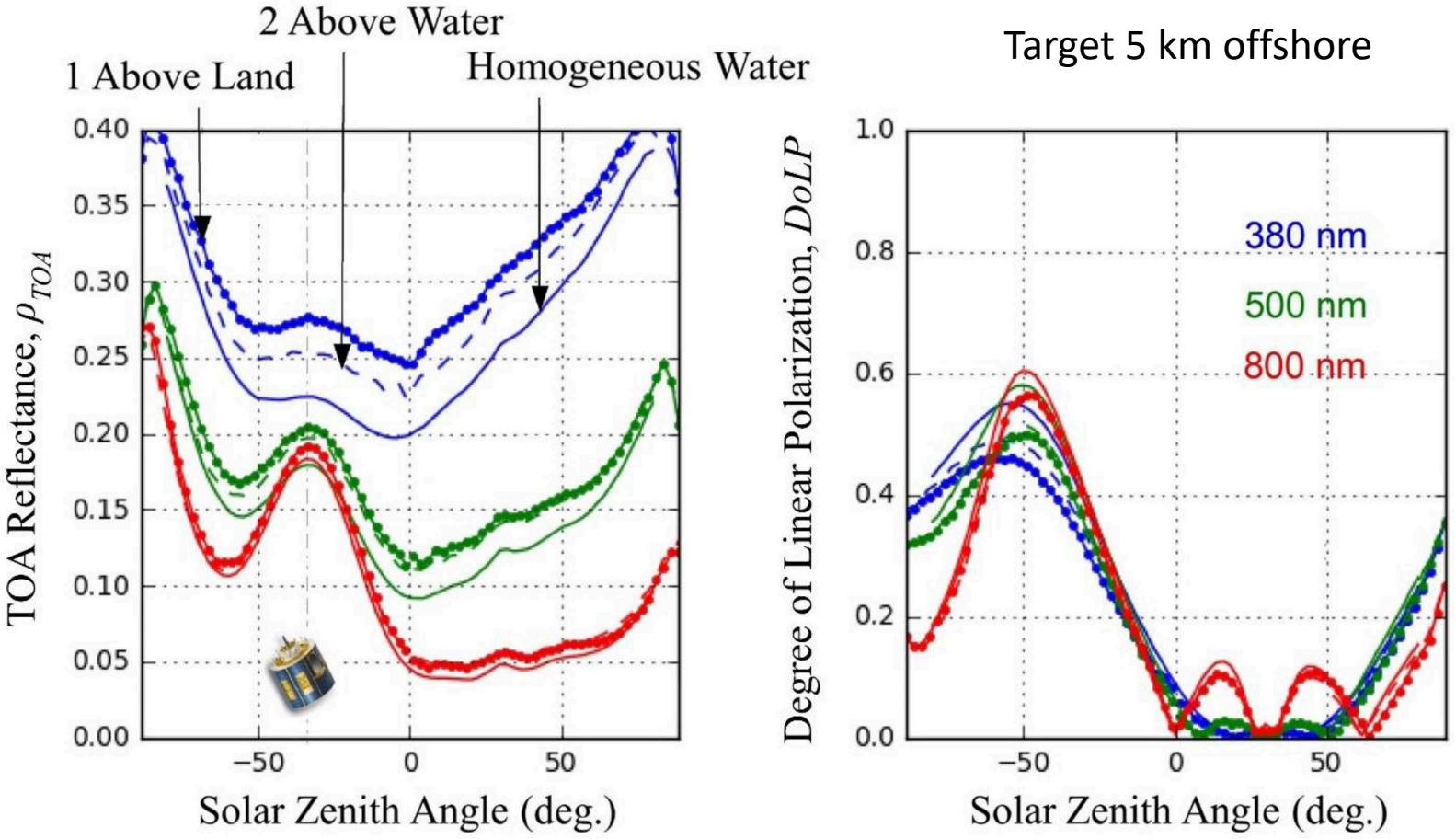

-Due to adjacency effects TOA reflectance is increased, and degree of polarization is decreased, especially at 380 nm where atm. scattering is effective.

***Figure 3.2**: TOA reflectance and degree of polarization of a water target located 5 km from a linear coastline as a function of solar zenith angle. Viewing zenith angle is 30 deg. The land reflectance is 0.8 (snow). Results are displayed at 380, 500, and 800 nm in the principal plane of the Sun for the sensor above water and above land, and assuming no adjacency effect (homogeneous water). (After Frouin et al., 2019.)*

Impact on water reflectance retrieval

-Depending on the environment (e.g., vegetation, bare soil, ice, etc.), the coupling between surface reflection and atmospheric scattering may either decrease or increase the retrieved water reflectance with increasing wavelength.

-This spectral dependence is not captured by determining the atmospheric signal from measurements in the near infrared and extrapolating to shorter wavelengths.

MERIS, 4 March 2003, $\rho_w(560)$

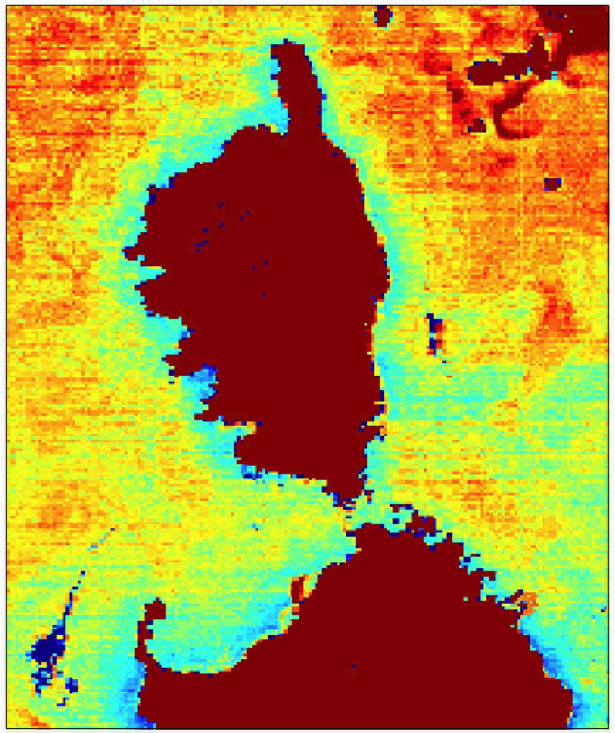

MERIS, 4 July 2008, $\rho_w(560)$

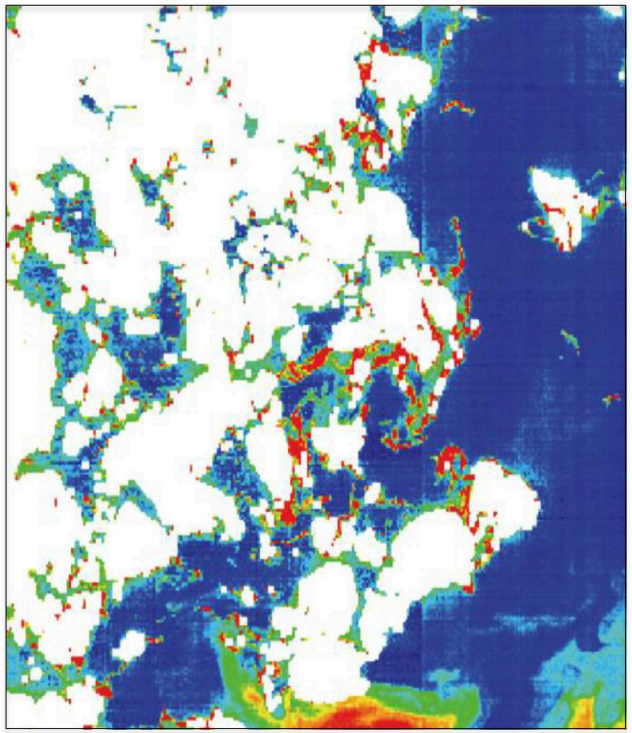

***Figure 3.3**: Marine reflectance at 560 nm retrieved from MERIS imagery acquired at 1 km resolution on 4 March 2003 over the Mediterranean Sea (left) and on 4 July 2008 over the Beaufort Sea (right). Standard MEGS processing was used. Values are anomalously low (blue/green pixels) over a distance of more than 10 km along the coast of Corsica and Northern Sardinia (left), and anomalously high (green/red pixels) near sea ice (right). This is attributed to the adjacency effect in the near infrared bands used for the correction of aerosol scattering.*

Impact of chlorophyll concentration retrieval

-The resulting errors on the retrieval of chlorophyll concentration may be large, even at distances of 20 km from the coast, as shown theoretically by Santer and Schmechtig (2000).

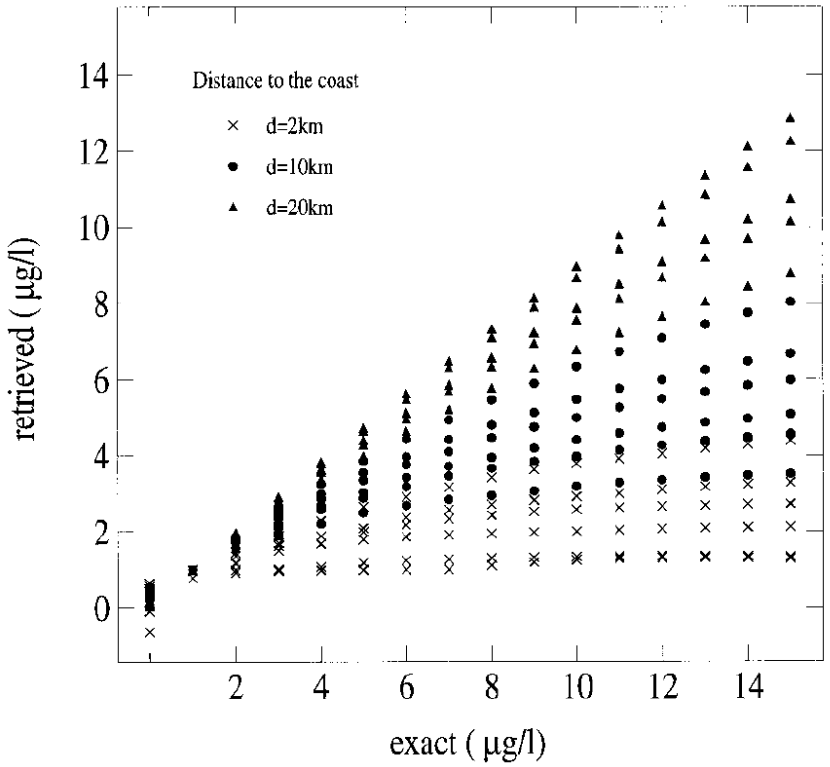

Figure 3.4: Impact of adjacency effect on the retrieval of chlorophyll-a concentration, C. Contrast between land and ocean reflectance is 0.3 at 865 nm and 0.07 at 670 nm.

-*A C* of 2 mg/m^3 is underestimated by 25% at a 10 km distance from shore when the atmospheric visibility is 23 km and 50% when the visibility is 8 km. The underestimation becomes larger as *C* increases, with retrieved values 5 times smaller than actual values at 10 mg/m^3 when the visibility is 8 km.

Formulation of the adjacency effect

-Homogeneous surface

$\rho_t \approx \rho_a + \rho_w T_a(\theta_s) T_a(\theta_v)/(1 - \rho_w S_a)$

-Heterogeneous surface

$\rho_t^* \approx \rho_a + T_a(\theta_s)[\rho_w \exp(-\tau_a/\cos(\theta_v)) + \rho_e t_a(\theta_v)]/(1 - \rho_e S_a)$

ρ_e: equivalent reflectance of the environment

-Adjacency effect:

$\Delta\rho_t = \rho_t^* - \rho_t \approx (\rho_e - \rho_w) t_a(\theta_v) T_a(\theta_s)$

-Environment reflectance

$$\rho_e = \int_{-\infty}^{+\infty} \int_{-\infty}^{+\infty} \rho_s(x,y)P(x,y)dxdy$$

P(x,y): Atmospheric point-spread function (expresses the contribution to the measured reflectance of surface-leaving photons scattered in the field of view).

-For small θ_v's (<30 deg.), P(x,y) ≈ P(r)

$$\rho_e = (1/2\pi) \int_0^{2\pi} \int_0^{+\infty} \rho_s(r,\phi)\,[dF(r)/dr]drd\phi$$

$F(r) \approx [t_{am}F_m(r) + t_{ap}F_p(r)]/(t_{am} + t_{ap})$

$F_m(r) = A_m[0.93exp(-0.08r) + 0.07exp(-1.1r)]$

$F_p(r) = A_p[0.037exp(-0.02rH_0/H) + 0.62exp(-1.8rH_0/H)]$

H: Scale height of aerosols; H_0 = 2 km; r in km.

A_m, A_p: Normalization factors

Variability of the adjacency effect

-The adjacency effect produced by molecular scattering and aerosol scattering are different and vary with F and the reflectance of the background.

1.The scales of influence are different. F_m exhibits an exponential decay with a scale of 12 km, while F_p has a far more rapid decrease with a scale of less than 1 km.

2. Molecular scattering varies with wavelength and increases very rapidly in the blue, but F_m remains about the same with a good approximation.

3. Aerosol scattering is less spectrally selective, but changes in the aerosol physical properties like the size distribution would modify its single scattering phase function and the coefficients of the exponential decrease with distance.

4. The spread is larger if the aerosols are at a higher altitude.

How to handle adjacency effects?

-One way to deal with adjacency effects is to develop atmospheric correction algorithms that minimize the effects.

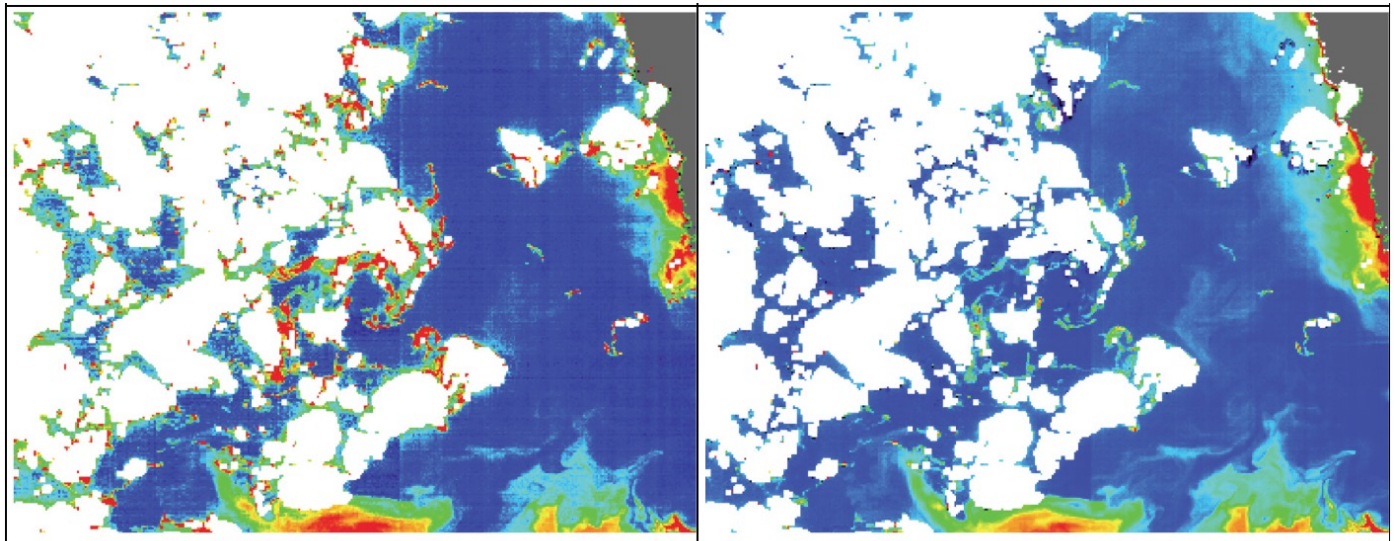

Water reflectance at 560 nm, MEGS processing (detail)	Water reflectance at 560 nm, POLYMER processing (detail)
Beaufort Sea, 2008-07-04, MERIS	

Figure 3.5: MERIS image of the Beaufort Sea showing that the standard processing is affected by the ice environment, leading to an anomalous increase of retrieved reflectance (left). Adjacency effects are reduced with the POLYMER algorithm (Steinmetz, 2011), which models the atmospheric signal as a polynomial function of the wavelength ($C_0 + C_1\lambda^{-1} + C_2\lambda^{-4}$).

Norwegian Coast, 4 July 2003, MERIS

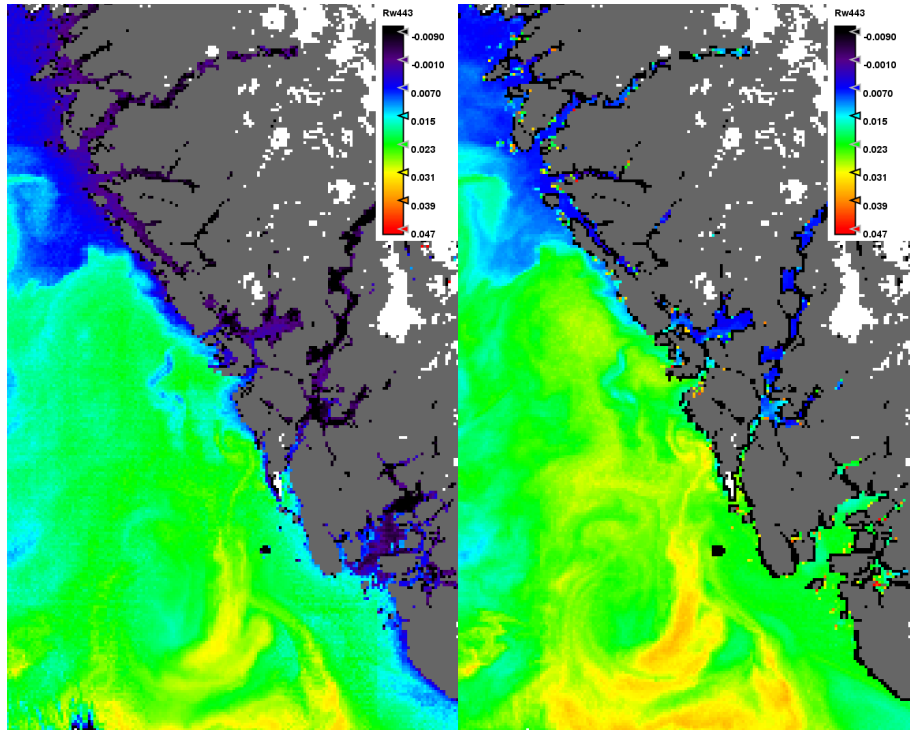

$\rho_w(443)$, MEGS $\rho_w(443)$, POLYMER

Figure 3.6: MERIS image of water reflectance at 443 nm (Norwegian Coast, 4 July 2003) showing that anomalously low reflectance near shore is well corrected for adjacency effects with the POLYMER algorithm.

-Another way is to correct systematically the TOA imagery for the adjacency effect at the Level 1b and produce a Level 1c, so that the processing of Level 2 products can be done by assuming that the surface is homogeneous (i.e., using the large target formalism of standard atmospheric correction schemes).

-The simplest option, easy to implement, is to correct only the adjacency effects associated with molecular scattering.

-A second option, more accurate, is to correct also the effects associated with aerosol scattering. This can be done:

(1) by assuming background aerosols or using aerosols with average properties (eventually seasonally and regionally dependent), and

(2) by estimating the aerosol properties (optical thickness, type, and altitude).

-In the case of clouds, one can assume that they are located at the surface, or one can estimate their altitude.

Example of adjacency correction (open ocean)

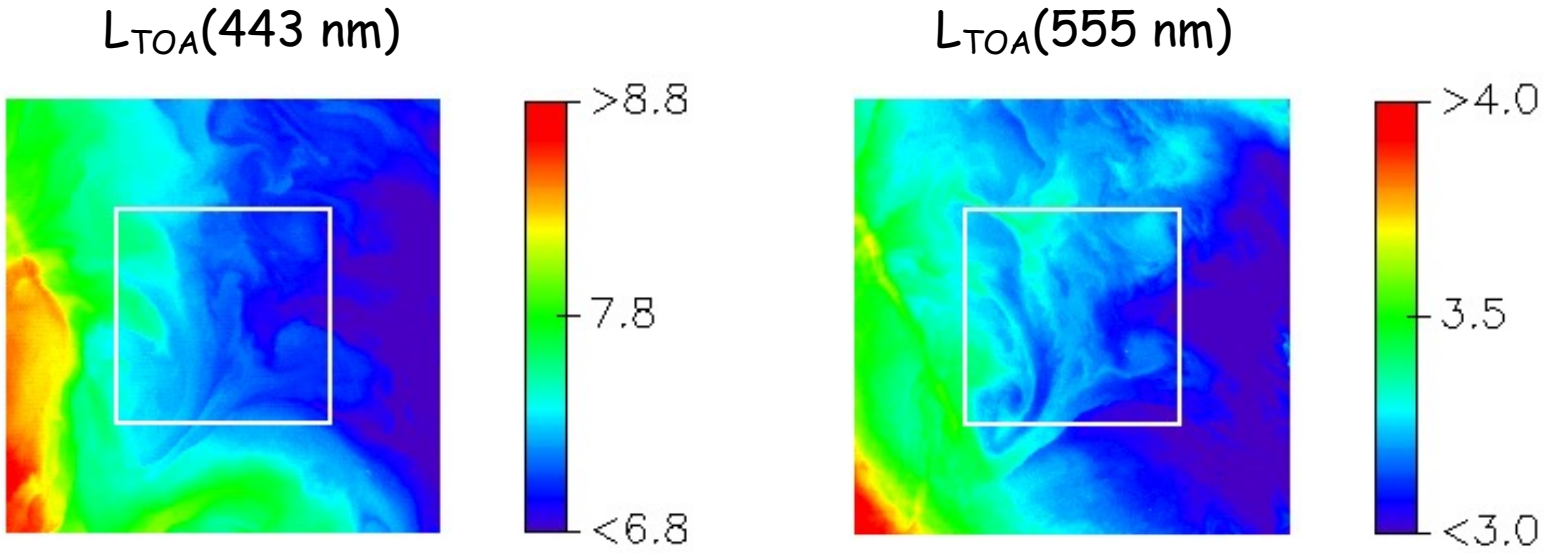

***Figure 3.7**: SeaWiFS LAC images of TOA Level 1b radiance at 443 and 555 nm (mW/cm²/µm/sr) obtained on 14 February 1999 in upwelling region off the coast of Namibia. The image is about 200x200 km in size. White rectangle denotes area within which adjacency effects are estimated.*

-Adjacency correction of spectral bands used for ocean color, i.e., 443 and 555 nm, was performed according to previous (simplified) equations for ρ_e and F using the aerosol content derived from the operational atmospheric correction algorithm. Aerosol scale height was fixed at 2 km.

Impact on water reflectance and chlorophyll-a concentration

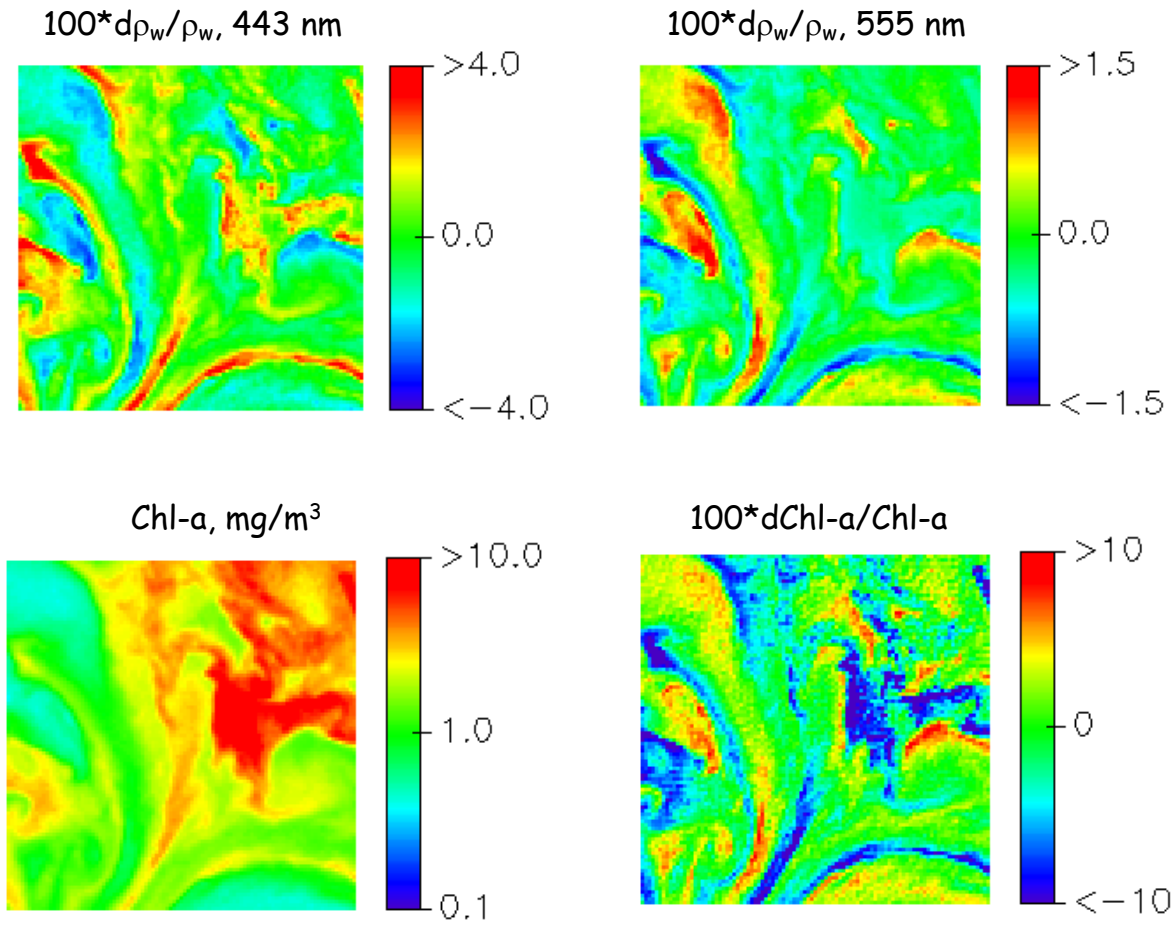

Figure 3.8: (Bottom left) Chlorophyll-a concentration computed from marine reflectance at 443 and 555 nm, after correction for adjacency effects. (Bottom right) Error on chlorophyll-a concentration due to adjacency effects. (Top left and top right) Error on marine reflectance at 443 nm and 555 nm due to adjacency effects.

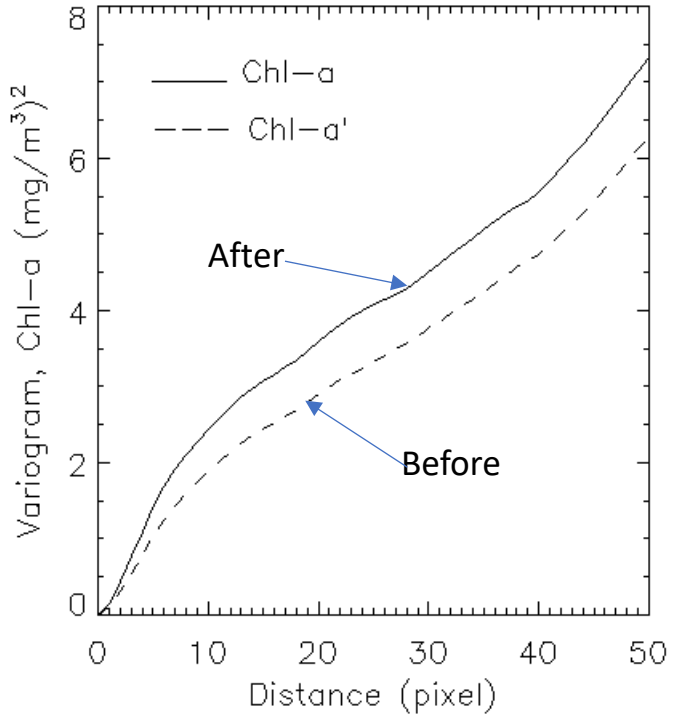

Figure 3.9: Variogram of chlorophyll-a concentration. Spatial correlation is changed significantly (influence of local processes is comparatively decreased at large scales after correction of adjacency effects).

-Even in open ocean, adjacency effects may be significant.

Conclusions about AC in the presence of adjacency effects

-The adjacency effect can be important, not only in the coastal zone or in the vicinity of sea ice and clouds, but also in the open ocean (e.g., in upwelling regions).

-Non negligible errors in the retrieval of chlorophyll-a concentration (>10% in the typical example considered) and a significant change in spatial structure, correlation scales.

-Correcting systematically Level 1b imagery for the adjacency effect is recommended. For coarse resolution sensors like MODIS, VIIRS, OCI, it may be sufficient to correct the effect due to molecular scattering (F associated with aerosols decreases exponentially with a scale of 1 km).

-As a result, the accuracy, quality, and daily coverage of aerosol and ocean-color products should be improved substantially over water surfaces contiguous to land surfaces, sea-ice, and clouds, and where spatial variability is relatively large.

4. Clouds/Sun glint

Introduction

-It is currently admitted that ocean color can be observed from space only over cloud-free and Sun glint-free areas.

-In the state-of-the-art algorithms, the presence of a cloud or even a minimum amount of Sun glint prevents utilization of the data.

-Consequently, the daily ocean coverage is typically 15-20%, and weekly products show no information in many areas.

-This limits considerably the utility of satellite ocean color observations in oceanography. Global coverage is required every three to five days in the open ocean and at least every day in the coastal zone.

Statistics of TOA reflectance over ocean in near infrared

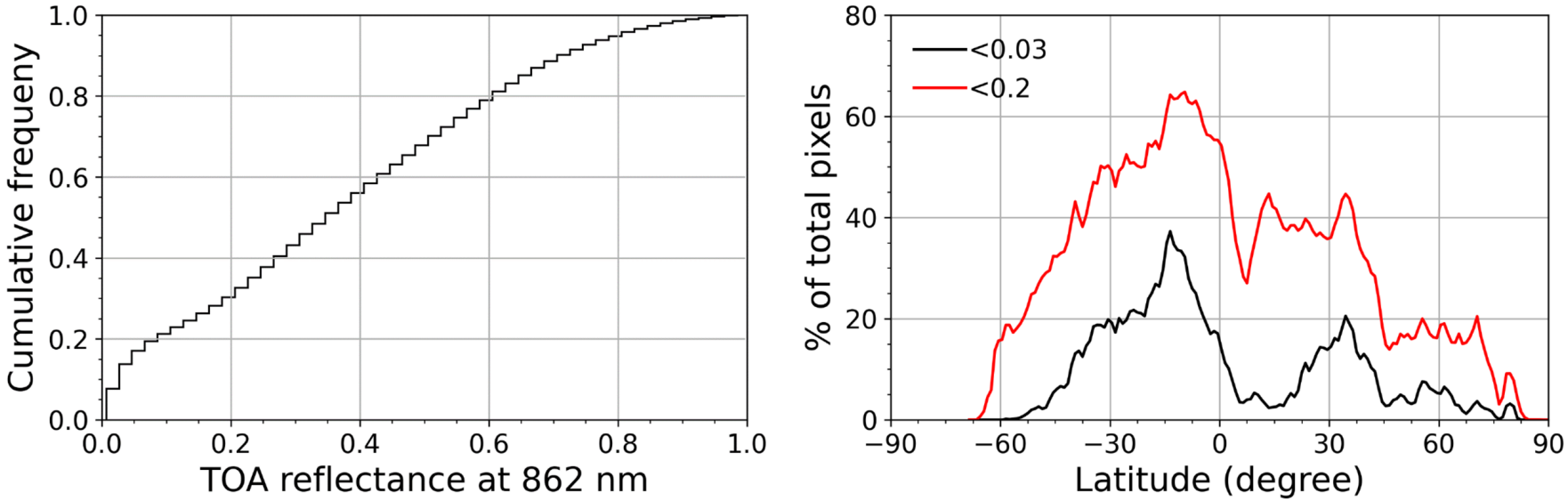

Figure 4.1. Left: Cumulative histogram of the TOA reflectance at 862 nm observed by VIIRS-SNPP over the global ocean on 15 July 2018; Right: Percentage of VIIRS-SNPP pixels (observations of 15 July 2018) selected by a threshold of 0.03 and 0.2 for the TOA reflectance at 862 nm.

-For a cloud albedo of 0.2, 80% of the photons that are incident upon on the top of the cloud layer may reach the surface, and 80% of the photons reflected by the ocean are transmitted back through the cloud layer. The transmittance along the double optical path through the cloud layer, 64%, is large, i.e., the signal measured at satellite altitude is sensitive to interactions with, and therefore to the characteristics of the water body.

RT simulations of TOA spectral reflectance, black water body

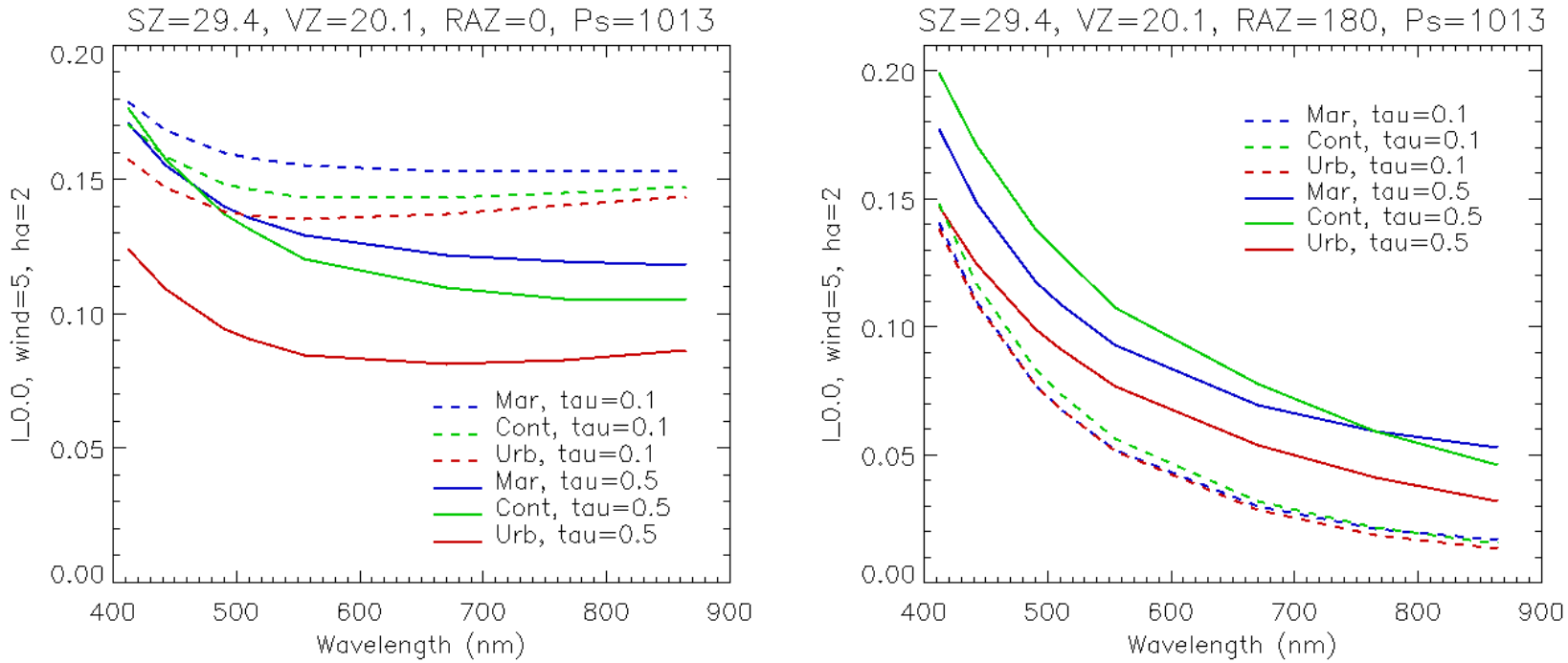

***Figure 4.2**: Simulations, using a successive-orders-of-scattering code, of the top-of-atmosphere normalized radiance in the solar plane for several aerosol conditions. Water body is black. (Left) Forward scattering. (Right) Backscattering.*

-Perturbing signal results from many processes and couplings, that may be difficult to model accurately. But importantly, it is smooth spectrally.

-Perturbing signal can be represented accurately by a polynomial or a linear combination of orthogonal components with a few terms or eigenvectors

$\rho_p(\lambda_i) \approx \sum_j [a_j \lambda_i^{nj}]$

$\rho_p(\lambda_i) \approx \sum_j [c_j e_{ji}]$

-Three n_j or e_j are usually sufficient.

-POLYMER spectral matching algorithm (Steinmetz et al., 2011) models the residual signal after correction for molecular scattering and some glint as:

$$\rho_{gam} = \rho_{TOA} - \rho_m - \rho_g = C_0 + C_1 \lambda^{-1} + C_2 \lambda^{-4}$$

-PCA-based algorithm (Gross et al., 2007) combines PCs of TOA signal sensitive to ocean signal retrieve PCs of water reflectance, allowing reconstruction of the marine reflectance.

$$\rho_{TOA} = \sum_i c_{pi} \mathbf{e}_{pi} \qquad \rho_w = \sum_j c_{wj} \mathbf{e}_{wj} \qquad c_{wj} = g(c_{pi}\text{'s})$$

POLYMER retrieval, MERIS, 21 June 2005, NE Atlantic

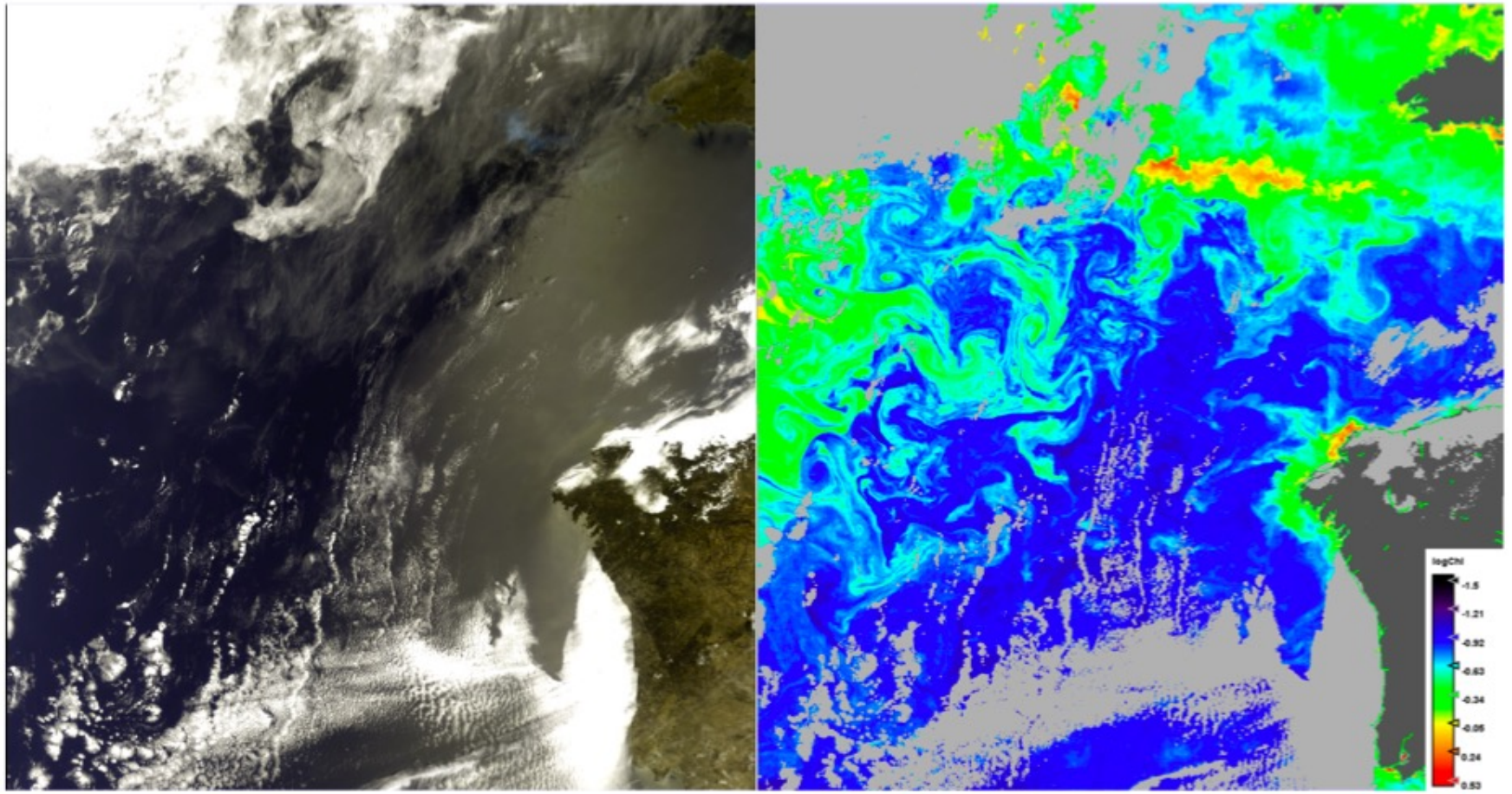

***Figure 4:3**: RGB composite of a MERIS scene off Portugal, 21 June 2005 (left) and chlorophyll concentration derived by the POLYMER algorithm (right). Chlorophyll concentration is retrieved in the presence of thin clouds and sun glint, and the chlorophyll patterns exhibit spatial continuity from cloud- and glint-free areas to adjacent cloud- and/or glint-contaminated areas. (After Steinmetz et al., 2011.)*

POLYMER vs MEGS, 21 December 2003

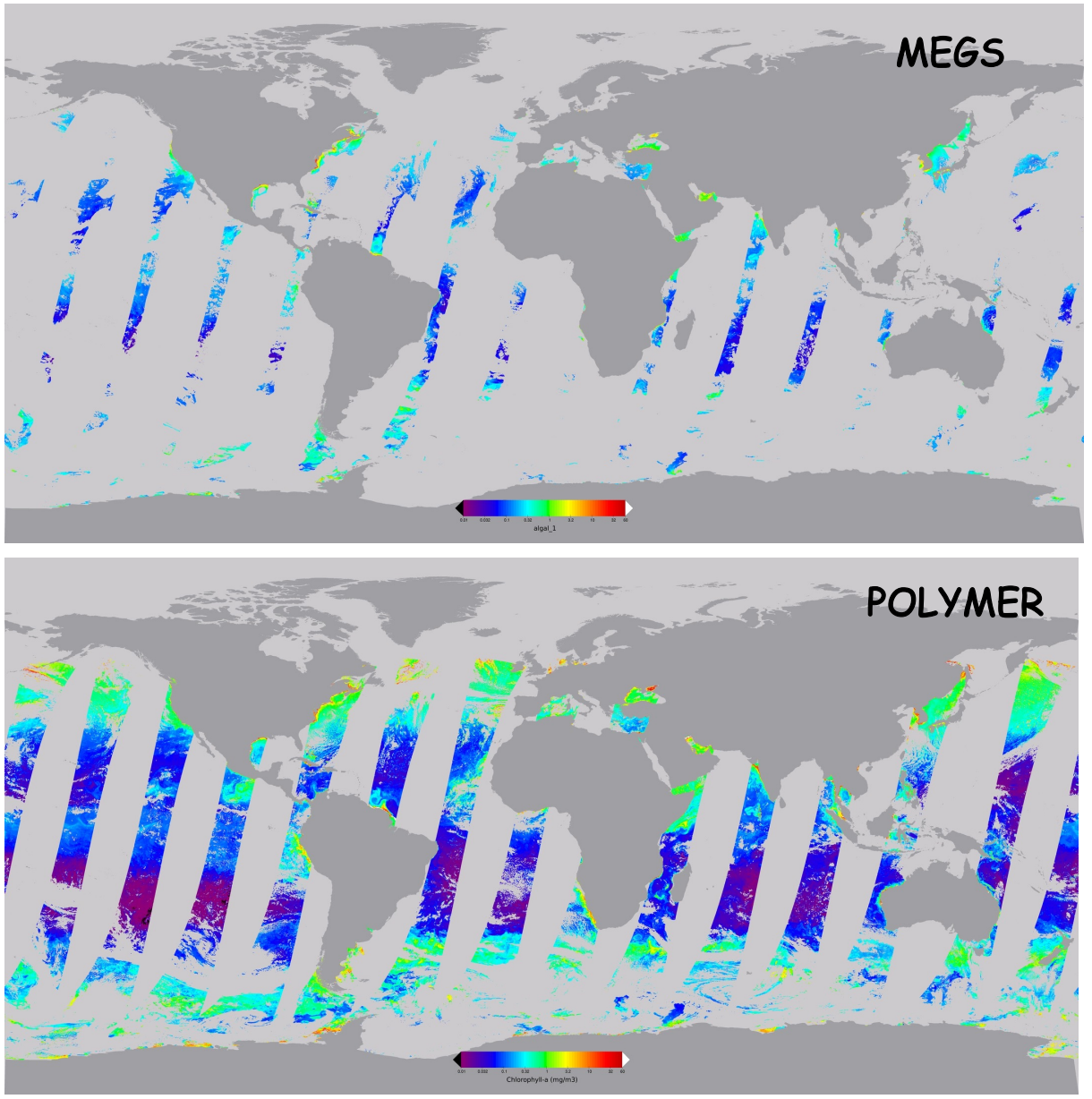

-Daily global coverage is dramatically increased using POLYMER. Good spatial continuity between glint-contaminated and glint-free areas.

***Figure 4.4**: MERIS level 2 imagery of POLYMER-derived chlorophyll concentration, 21 December 2003.*

POLYMER vs MEGS and standard OBPG AC, 3-day composite, 3-5 June 2003, Arabian Sea

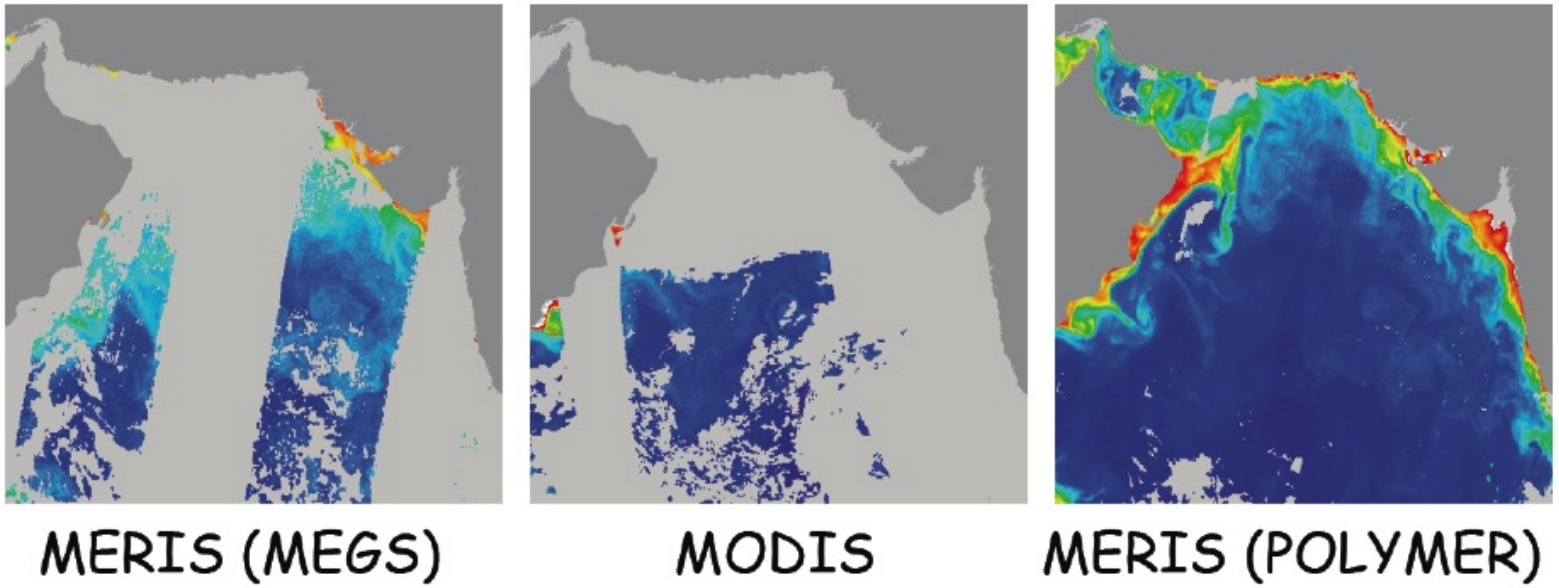

***Figure 4.5**: Level 3 composites of chlorophyll concentration, 3 to 5 June 2003, in the Arabian Sea, showing a dramatic increase in spatial coverage by the POLYMER algorithm.*

-Spatial coverage is increased from 26% (MODIS/Standard) to 49% (MERIS/MEGS) and 92% (MERIS/POLYMER)

PCA-based Retrieval, 21 June 2005, Northeast Atlantic

RGB

ρ_w(443 nm)

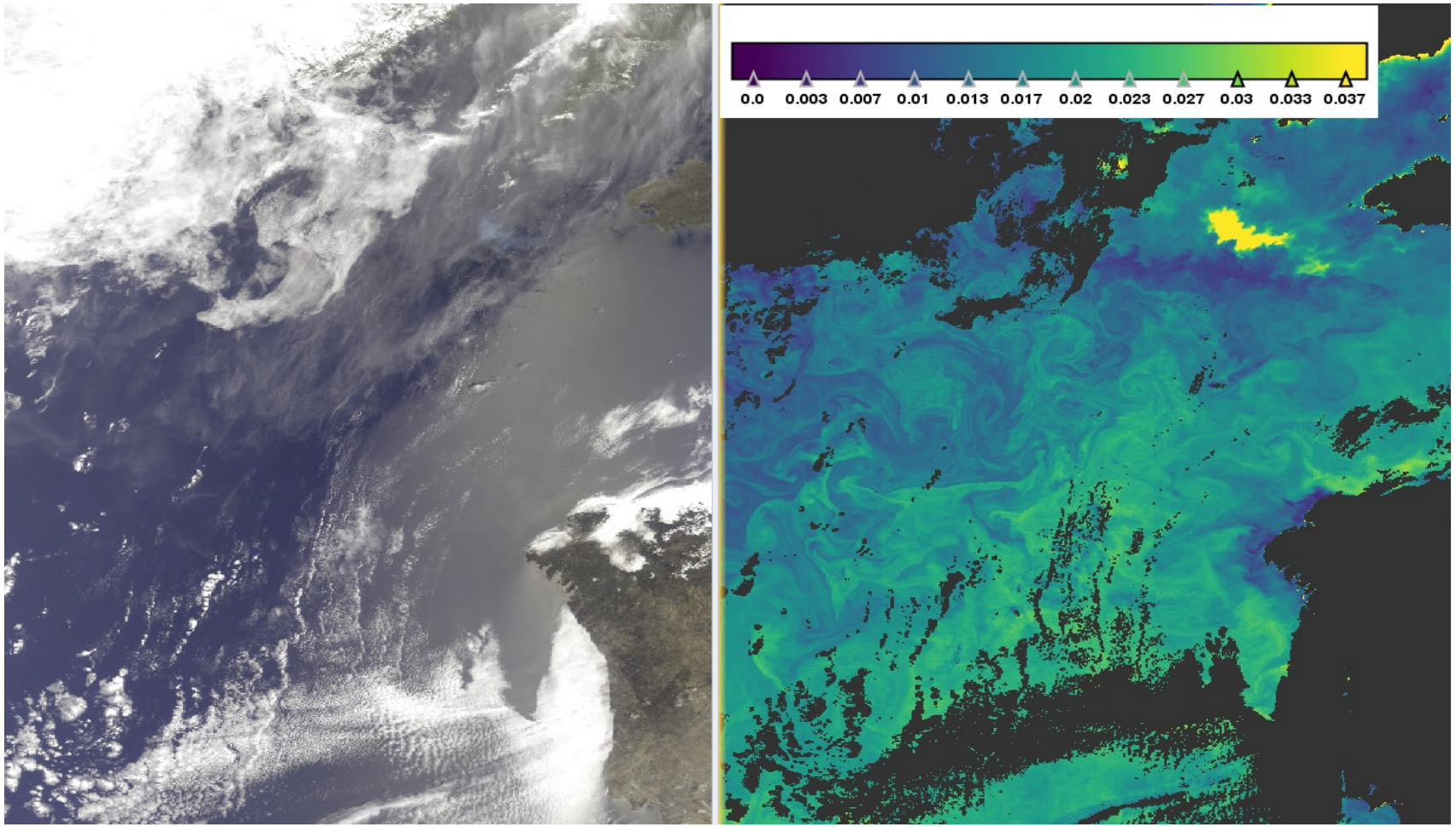

***Figure 4.6**: Same as Figure 1 but PCA-based algorithm and, instead of chlorophyll concentration, marine reflectance at 443nm (R. Frouin and L. Gross, unpublished.)*

PCA-Based retrieval, 09 November 2003, Arabian Sea

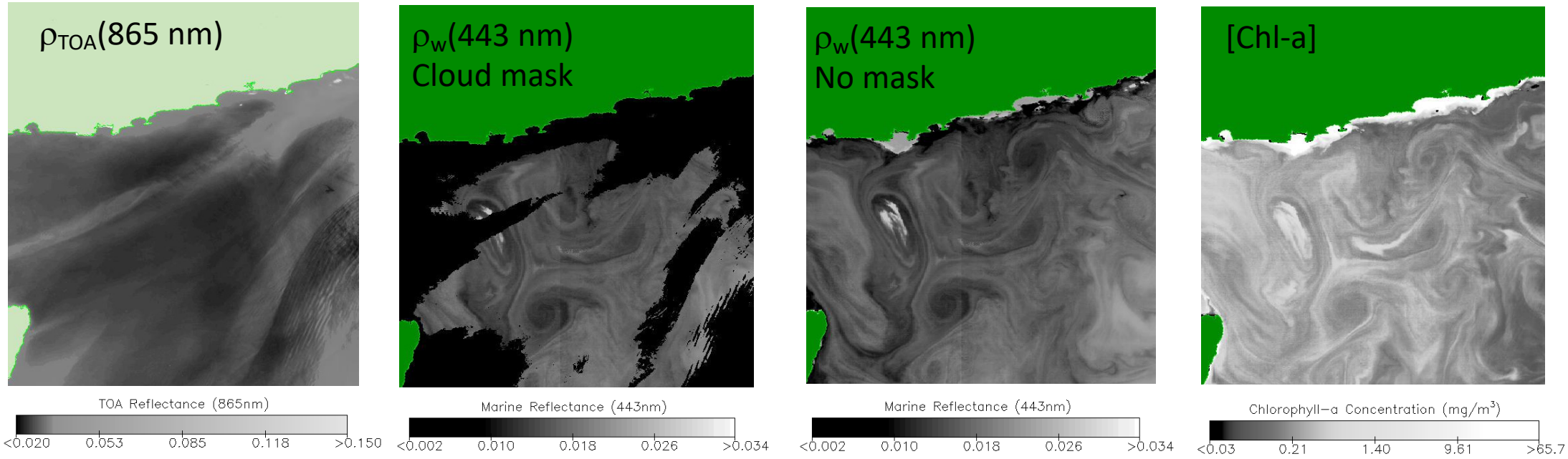

***Figure 4.7**: Imagery acquired by MERIS over the Arabian Sea on 09 November 2003. Left: Reflectance at 865 nm showing thin clouds. Center left: Retrieved marine reflectance (PCA-based algorithm) with standard threshold of 0.03 at 865 nm. Center right: Same as center left, but threshold of 0.2 at 865 nm. Right: Retrieved chlorophyll-a concentration with threshold of 0.2 at 865 nm. (R. Frouin and L. Gross, unpublished.)*

-One may use PCs of the TOA signal directly to predict, via machine learning, ocean color properties derived from the MODIS atmospheric correction algorithm (Fasnacht et al., 2022).

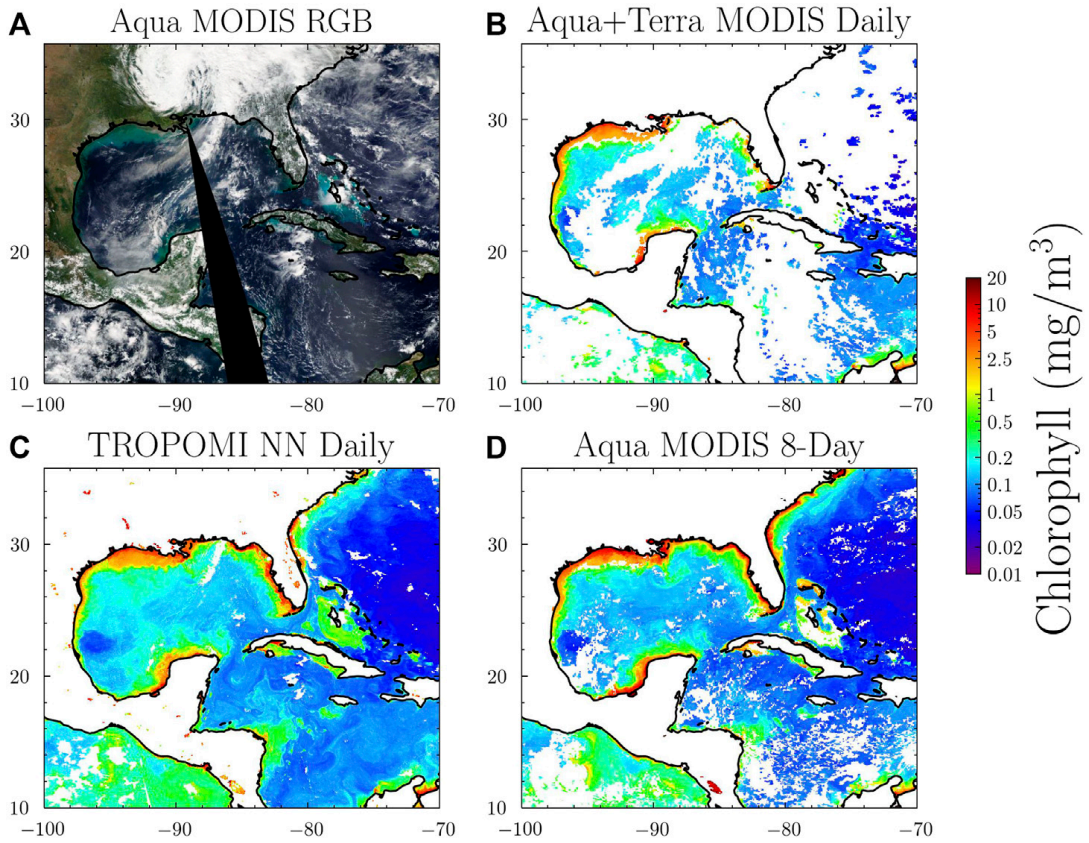

***Figure 4.8**: Chlorophyll retrievals in the Gulf of Mexico for 10 October 2020. (A) shows a true color image from MODIS Aqua, (B) shows MODIS-Aqua daily 4 km retrieval, (C) shows TROPOMI machine learning-based chlorophyll, and (D) shows MODIS-Aqua 8-day composite of chlorophyll.*

-Neural network is trained to predict ocean color properties for OMI/TROPOMI pixels that are co-located with the MODIS retrievals of R_{rs} and chlorophyll.

-Assumption is that MODIS retrievals are correct.

-TROPOMI machine learning approach yields very few gaps in coverage. No noticeable contamination in the TROPOMI chlorophyll from Sun glint features.

Conclusions about AC in the presence of clouds and Sun glint

-Atmospheric correction of satellite ocean-color imagery can be performed through thin clouds and in the presence of Sun glint.

-The POLYMER, PCA-based, and machine learning algorithms yield imagery that is comparable with standard imagery. Spatial continuity is good from cloud- and glint-free areas to adjacent cloudy and/or glint-affected areas. Daily ocean coverage, 15-20% with standard algorithms, is increased substantially.

-Machine learning based on satellite retrievals may yield robust retrievals (large training set) but assumes that satellite-derived products are the reference.

-The gain in coverage allow one to resolve better phytoplankton blooms in the open ocean and "events" linked to wind forcing in the coastal zone. This could lead to important new information about the temporal variability of biological processes.

5. Other Issues

-Radiometric calibration

-Spatial heterogeneity of atmosphere

-Aerosol altitude

-Earth curvature

-Separation of CDOM and aerosol absorption in UV

Aerosol altitude

-May have a significant effect on the TOA signal even when aerosols are not absorbing, simply due to the coupling between aerosol and molecule scattering, which depends on the relative altitude of the scatterers.

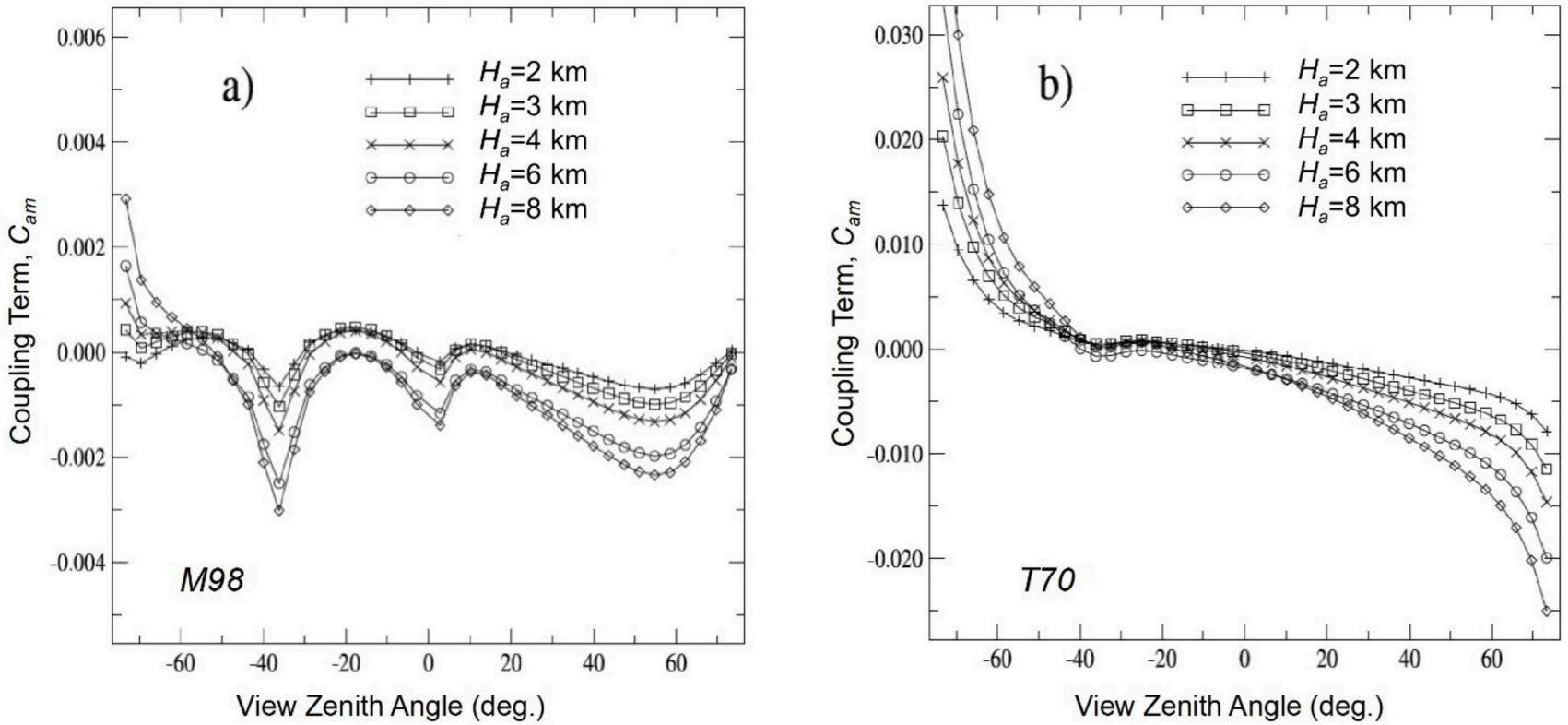

-For some viewing angles, the effect of neglecting aerosol scale height variability reaches 0.002 (M98) and over 0.01 (T70) in amplitude, which for T70 is an order of magnitude larger that accuracy requirements).

***Figure 4.9**: Effect of aerosol altitude, Ha, on the coupling term, Cam, of the atmospheric reflectance due to interactions between aerosol and molecular scattering. Wavelength is 443 nm and aerosol models are M98 (a) and T70 (b). Aerosol optical thickness is 0.1 at 865 nm. Solar zenith angle is 36.2 . Results are for the principal plane (negative zenith angles correspond to backscattering). The case of Ha = 8 km corresponds to homogeneously mixed aerosols and molecules. Reproduced with permission from the University of Lille, France (After Tieuleux, 2002).*

Earth curvature

-For solar zenith angles >70 deg. assuming that the Earth atmosphere is flat (i.e., plane-parallel) is a problem. A spherical-shell atmosphere is more appropriate. But even at small zenith angles, the error on molecular reflectance, a fraction of 1%, may significantly impact water reflectance retrievals.

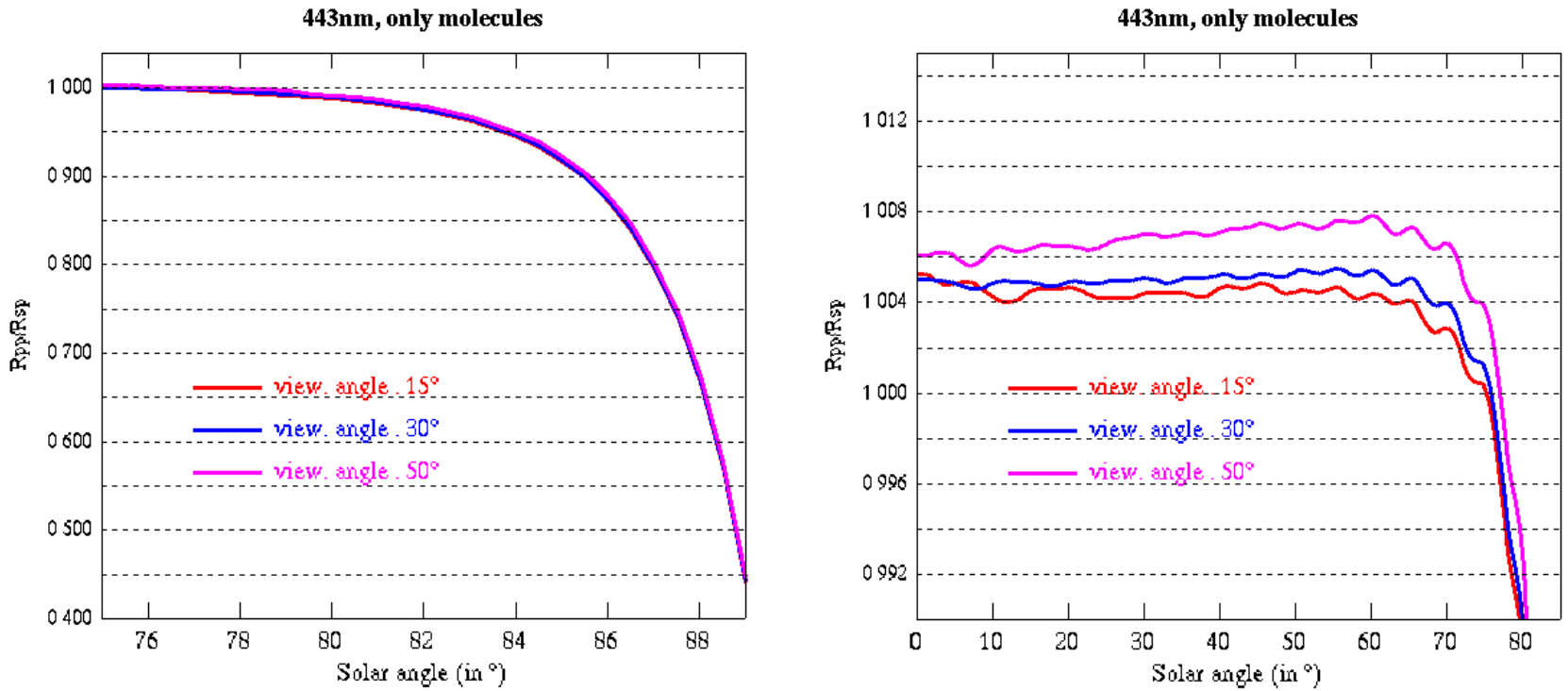

***Figure 4.10**: Ratio of the reflectance for spherical geometry over the reflectance for plane-parallel geometry for a pure molecular atmosphere over a black surface and for different viewing angles. (D. Jolivet, HYGEOS, personal communication.)*

Separation of CDOM and aerosol absorption in UV

-Spectral dependence of the aerosol and CDOM absorption effects may be comparable, making distinction of the two signals difficult in some one-step atmospheric correction schemes (e.g., spectral-matching).

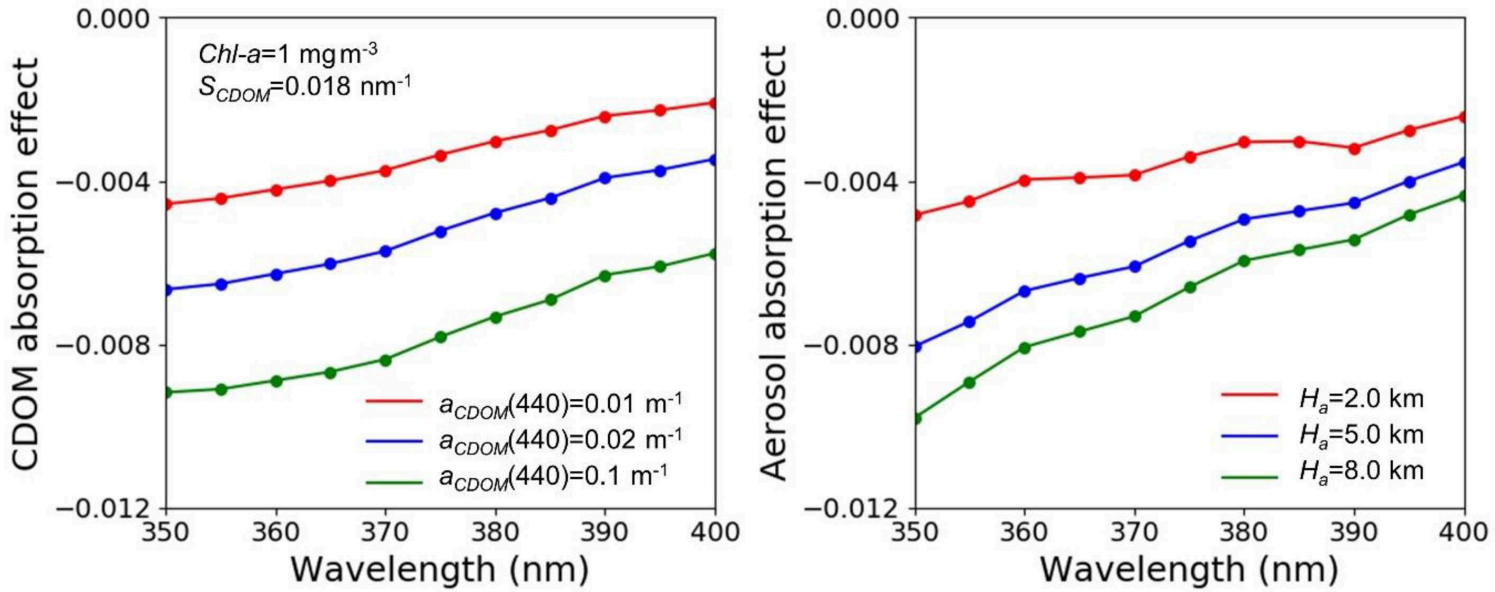

-CDOM absorption of 0.01 m^{-1} has nearly the same effect as aerosol absorption when scale height is 2km, i.e., about −0.002 over 50 nm.

Figure 4.12: (Left) Simulated CDOM absorption effect on water signal at top of atmosphere, for CDOM absorption coefficients of 0.01, 0.02, and 0.1 m^{-1}. Chlorophyll-a concentration is 1 mgm^{-3}. (Right) Simulated aerosol absorption effect for scale heights of 2, 5, and 8 km. Spectral slope of CDOM absorption is 0.018 nm^{-1}. Aerosols are of maritime type with optical thickness of 0.2 at 550 nm and scale height of 2 km, and wind speed is 7 m s . Solar zenith angle is 30 deg., viewing zenith angle 15 deg., and relative azimuth angle 90deg. (After Frouin et al., 2019.)